



Characterization of Composite Cores for High Temperature-Low Sag (HTLS) Conductors

Final Project Report

Power Systems Engineering Research Center

*A National Science Foundation
Industry/University Cooperative Research Center
since 1996*



Characterization of Composite Cores for High Temperature-Low Sag (HTLS) Conductors

Final Project Report

Project Team

**Ravi Gorur, Project Leader
Barzin Mobasher
Arizona State University**

Robert Olsen, Washington State University

PSERC Publication 09-05

July 2009

Information about this project

For information about this project contact:

Ravi Gorur
Department of Electrical Engineering
Arizona State University
P.O. Box 875706
Tempe, AZ 85287-5706
Tel: 480-965-4894
Fax: 480-965-0745
Email: ravi.gorur@asu.edu

Power Systems Engineering Research Center

The Power Systems Engineering Research Center (PSERC) is a multi-university Center conducting research on challenges facing the electric power industry and educating the next generation of power engineers. More information about PSERC can be found at the Center's website: <http://www.pserc.org>.

For additional information, contact:

Power Systems Engineering Research Center
Arizona State University
577 Engineering Research Center
Tempe, Arizona 85287-5706
Phone: 480-965-1643
Fax: 480-965-0745

Notice Concerning Copyright Material

PSERC members are given permission to copy without fee all or part of this publication for internal use if appropriate attribution is given to this document as the source material. This report is available for downloading from the PSERC website.

© 2009 Arizona State University and Washington State University
All rights reserved.

Acknowledgements

This is the final report for the Power Systems Engineering Research Center (PSERC) research project T-33 titled “Characterization of Composite Cores for High Temperature-Low Sag (HTLS) Conductors” We express our appreciation for the support provided by PSERC’s industrial members and by the National Science Foundation under grant NSF EEC-0001880 received under the Industry / University Cooperative Research Center program.

The authors wish to recognize their graduate students contributed to the research and creation of the reports: Sushil Shinde (Arizona State University), and Juan Erni (Arizona State University).

The authors thank all PSERC members for their technical advice on the project, especially the industry advisors for the project:

- M. Dyer & J. Hunt - Salt River Project
- J. Gutierrez - Arizona Public Service
- J. Robinson, Duke Energy

Executive Summary

New conductors that employ high strength light weight composite cores are being introduced in the electric power system to address the complex problems associated with increasing electric power transmitted with minimal new construction in existing right-of-ways. Two of these conductors are: aluminum carbon composite conductors (ACCC) and aluminum conductor composite reinforced (ACCR) conductors. The ACCR conductor uses a metal matrix core and the ACCC conductor uses a carbon composite core. Composite cores have a higher strength and lower coefficient of thermal expansion when compared with the steel core used in traditional aluminum conductor steel reinforced (ACSR) conductors.

The literature published by manufacturers on these conductors indicates that they are stable for continuous use in the range 150-210 °C, as compared to 100 °C for traditional ACSR conductors. Published emergency ratings allow a conductor temperature of 240 °C. These claims must be validated for these conductors to be accepted as viable replacement of traditional overhead conductors employing a steel core.

The effect of the temperature distribution on the current carrying capacity of these conductors is not known. The objective of this study is to model the radial temperature distribution and its effect on current carrying capacity in bare overhead ACCC and ACCR conductors. This study develops a method to calculate the radial temperature distribution in composite (ACCC & ACCR) conductors. The radial temperature of the conductor is derived from the general heat equation and the resultant heat transfer to the outside for composite conductors. The available mathematical models like “radial and axial temperate gradients in bare stranded conductor,” and “the radial temperature distribution and effective radial thermal conductivity in bare solid and stranded conductors,” were used for verification of results on ACSR conductors.

Based on the developed model, a comparative analysis was completed for Drake type ACSR, ACCR and ACCC conductors. Radial temperature distribution results were obtained for various values of current, emissivity, thermal conductivity of the conductor and ambient temperature. The thermal model predicts that the radial temperature difference in metal matrix conductor is less than that of carbon composite conductor. The radial temperature decreases as emissivity of conductor is increased. There is slight increase in radial temperature difference as ambient temperature increases. The study indicates that varying the thermal conductivity of the outer conducting material does not significantly affect the outer surface temperature. However it does have a slight effect on the radial temperature difference. This difference (18°C -20°C) is significant for ACSR conductors compared to ACCR (4°C -8°C) and ACCC (2°C -6°C) conductors.

The mechanical performance of the carbon composite and metal matrix cores was studied by conducting tension tests at two temperatures. A tension test fixture was developed for carbon composite cores. The experimental tensile data was modeled using a back-calculation procedure to measure effect of temperature and ageing on the strength of fibers based on a Weibull distribution. Measurements of core tensile strength at high temperatures were compared between carbon composite and metal matrix cores of the same diameter. At elevated temperatures the carbon composite cores show a 26% reduction in tensile strength, but still met the required value.

The analysis done in this thesis largely consisted of examining the performance of the composite cores at elevated temperature for Drake type conductors. The future works in a related area are:

- Role of long term elevated temperature on mechanical strength
- In depth study of mechanisms leading to reduction in mechanical strength
- Validation of theoretical model results
- Correlation between formulation and processing on the cracking of carbon composite core.

Table of Contents

1. Introduction.....	1
1.1 Project Objectives.....	1
1.2 Motivation and Background.....	1
1.3 Previous Work.....	2
1.4 Thermal Rating of Bare Overhead Conductors.....	4
1.5 Organization of the Report.....	5
2. Thermal Ageing of Composite Conductors.....	6
2.1 Introduction.....	6
2.2 Composite Conductors.....	6
2.3 Thermal Stress of the Carbon Composite Core.....	7
2.4 Experimental Results for Metal Matrix and Carbon Composite Core.....	9
3. Calculating the Current-Temperature of Bare Overhead Conductors.....	12
3.1 Introduction.....	12
3.2 Steady-State Heat Balance.....	12
3.3 Computer Program for Thermal Rating.....	15
3.4 Results.....	19
3.5 Conclusion.....	23
4. Radial Temperature Distribution in Composite Conductors.....	24
4.1 Introduction.....	24
4.2 Conduction Equation for Overhead Conductor.....	24
4.3 Computer Model.....	26
5. Study of IEEE Standard – 738 for Calculating the Current-Temperature of Bare Overhead Conductors.....	34
5.1 Introduction.....	34
5.2 Test Setup and Procedure.....	34
5.3 Test Results.....	40
5.4 Analysis of Test Results.....	41
5.5 Weibull Statistics.....	44
6. Conclusions and Future Work.....	50
6.1 Conclusions.....	50
6.1 Future Work.....	50
References.....	51

List of Figures

Figure 1.1: Typical ACSR conductor	4
Figure 2.1: Aluminum conductor.....	7
Figure 2.2: Aluminum conductor.....	7
Figure 2.3: The cross-section of a new carbon composite core sample.....	7
Figure 2.4: The cross-section of the sample kept in furnace for 5 days at 175 °C	8
Figure 2.5: The cross-section of the sample kept in furnace for 15 days at 200 °C	8
Figure 2.6: An aged sample showing the polymer resin of the carbon composite core	9
Figure 2.7: SEM image of a metal matrix core subjected to 210 °C for 120 hrs and virgin sample.....	9
Figure 2.8: SEM image of a carbon composite core subjected to 210 °C for 120 hrs and virgin sample	10
Figure 2.9: SEM image of a carbon composite core subjected to 210 °C for 120 hrs and virgin sample.....	10
Figure 2.10: Cracking in resin of carbon composite when subjected to 240 °C for 120 hrs.....	11
Figure 3.1: Conductor temperature vs. time curve for base case 1.....	19
Figure 3.2: Conductor temperature vs. time curve for case 3.....	20
Figure 3.3: Temperature vs. time curve for case 4 (change in sun time 12 hr)	20
Figure 3.4: Temperature vs. time curve for case 5 (change in sun time 18hr)	21
Figure 3.5: Temperature vs. time curve for case 6 (change in day of the year, NDAY=250)	21
Figure 3.6: Temperature vs. time curve for case 7 (change in day of the year, NDAY=365)	22
Figure 3.7: Temperature vs. time curve for case 8 (change in velocity of wind, 1 m/s) ..	22
Figure 3.8: Temperature vs. time curve for case 9 (change in velocity of wind, 0 m/s) ..	23
Figure 4.1: Typical composite conductor	24
Figure 4.2: Surface temperature T_c and core temperature T_s as a function of current.....	29
Figure 4.3: Radial temperature difference as a function conductor current	30
Figure 4.4: Temperature as a function of the emissivity (E) at conductor current $I=1000A$	31
Figure 4.5: Temperature as a function of thermal conductivity of the outer conducting material at $I=1000A$	32
Figure 4.6: Temperature as a function of an ambient temperature (T_a) for $I=1000A$	33

Figure 5.1: Tensile testing system	35
Figure 5.2: Schematic diagram of test system	35
Figure 5.3: 3-D view of a main body of cylindrical grip	36
Figure 5.4: End cap of cylindrical grip	36
Figure 5.5: Cylindrical grip with tapered wedge	36
Figure 5.6: Carbon composite core with cylindrical grips.....	37
Figure 5.7: Carbon composite core tensile test setup	37
Figure 5.8: Carbon composite core with rectangular grip with wedge in split end grip tool	38
Figure 5.9: Tensile test setup at elevated temperature.....	39
Figure 5.10: Tensile test failed samples with different grips.....	41
Figure 5.11: Test failure due to one of the wedge slipping from cylindrical grip	42
Figure 5.12: Stress-Strain curve at room temperature	42
Figure 5.13: Stress-Strain curve at elevated temperature	43
Figure 5.14: Comparison of Stress-Strain curve for two temperatures	43
Figure 5.15: Failure probability curve for carbon composite core	46
Figure 5.16: Weibull stress-strain curve for carbon composite core	47
Figure 5.17: Axial stress distribution for carbon composite core,.....	47
Figure 5.18: Failure probability curve for carbon composite core (for different values Weibull Modulus, m)	48
Figure 5.19: Weibull stress-strain curve for carbon composite core	49

List of Tables

Table 3.1: Case description for Table 3.2	16
Table 3.2: Inputs for conductor temperature (IEEE Standard 738-2006).....	16
Table 3.3: Case description for Table 3.4	17
Table 3.4: Inputs for conductor temperature (IEEE Standard 738-2006).....	17
Table 3.5: Results for conductor temperature (IEEE Standard 738-2006).....	18
Table 3.6: Results for conductor temperature (IEEE Standard 738-2006).....	18
Table 4.1: Typical overhead conductor characteristics.....	28
Table 5.1: Tensile test results.....	40
Table 5.2: Typical Weibull modulus (m) values for materials in fibrous form (inspired from [16])	48

Nomenclature

A	Conductor cross sectional area, m^2
A	Cross sectional area including air gaps, m^2
A'	Projected area of conductor, <i>square feet per linear foot</i>
A_m	Cross sectional area excluding air gaps, m^2
AAAC	All Aluminum Alloy Conductor
ACCC	Aluminum Carbon Composite Conductor
ACCR	Aluminum Conductor Composite Reinforced
ACIR	Aluminum Conductor Invar Reinforced
ACSR	Aluminum Conductor Steel Reinforced
ACSS	Aluminum Conductor Steel Supported
Al	Aluminum
$C1, C2$	Constants of integration
$C3, C4$	Constants of integration
CIGRE	International council on large electric systems (in English)
D	Conductor diameter, <i>in</i>
E	Modulus
H_c	Altitude of sun, <i>degrees</i>
HTLS	High Temperature Low Sag
Hz	Hertz
I	Total current flowing through conductor in Ampere
IEC	International Electrotechnical Commission
IEEE	Institute of Electrical and Electronics Engineers
J_0	The zero order Bessel functions of the first and second kind
K_a	Ambient temperature, $^{\circ}K$
K_{angle}	Wind direction factor
K_c	Temperature of conductor, $^{\circ}K$
k_g	Thermal conductivity of fiber glass material
KCM	Thousand Circular Mil
<i>kips</i>	Kilo Pounds
kN	Kilonewton
L	Length of fiber, m
lb	Pound
lbf	Pounds of Force
L_0	Gauge length
LVDT	Linear Variable Displacement Transducer
m	Weibull modulus
<i>mph</i>	miles per hour
MPa	Mega Pascal
P	Weibull probability
PSERC	Power Systems Engineering Research Center
<i>psi</i>	Pounds per Square Inch
q_c	Convection heat loss, <i>w/ft</i>

q_{cc}	Heat transfer rate in the glass fiber material
q_r	Radiated heat loss, w/ft
q_s	Heat gain from sun, w/ft
Q_s	Total solar and sky radiated heat flux, W/ft^2
r_{os}	Radius of composite core carbon material only, Ω
r_{sg}	Radius of composite core material (carbon + glass fiber) , Ω
R_{Tc}	60 Hz ac resistance of conductor at operating temperature T_c , Ω/ft
ROW	Right-of-ways
R_{sc}	Thermal resistance of carbon core material, Ω
R_{TC}	Resistance calculated at temperature T_C , Ω
R_{TL}	60 Hz ac resistance at temperature T_L , Ω
R_{TH}	60 Hz ac resistance at temperature T_H , Ω
T_a	Ambient temperature, $^{\circ}C$
T_c	Conductor temperature, $^{\circ}C$
T_C	Conductor temperature at which new 60 Hz resistance is desired, $^{\circ}C$
T_c	Temperature of the conducting material (conductor surface temperature), $^{\circ}C$
T_H	Conductor temperature at which the resistance R_{TH} is specified, $^{\circ}C$
T_L	Conductor temperature at which the resistance R_{TL} is specified, $^{\circ}C$
T_{sc}	Temperature of the carbon material layer in the core, $^{\circ}C$
T_{sg}	Temperature of the composite core (carbon + fiber glass), $^{\circ}C$
V_w	Wind speed, ft/hr
Y_0	The zero order Bessel functions of the first and second kind
Z_l	Azimuth of line, <i>degrees</i>
Z_c	Azimuth of sun, <i>degrees</i>
Zr	Zirconium
ε	Emissivity
Φ	Angle between wind and axis of the conductor, <i>degrees</i>
θ	Effective angle of incidence of the sun's rays, <i>degrees</i>
ρ_f	Density of air temperature T_f , $W/ft-^{\circ}C$
μ_f	Absolute viscosity of air temperature T_f , $lbs/ft-hr$
ρ_f	Density of air, lbs/ft^3
ρ	Electrical resistivity at 20 $^{\circ}C$
α	Temperature coefficient of resistance
σ	Stress in psi
σ_0	Characteristic fiber strength

1. Introduction

1.1 Project Objectives

The main objective of this study is to evaluate the effectiveness of composite cores used in overhead conductors at elevated temperatures. Primarily, study the effect of two temperatures on tensile strength and the radial temperature distribution in composite conductors. The short and long term exposure of composite core to high temperatures is a primary concern for the acceptance of these new overhead conductors. The operating temperature range of these conductors is expected to be 100 °C to 180 °C with short term maximum operating temperatures up to 200 °C. There is a concern about potential loss of strength due to matrix degradation and an attempt has been made to address this. This study focuses on the composite cores used in ACCR & ACCC conductors. They are referred in this document as Metal Matrix and Carbon Composite Cores.

This study seeks to develop a mathematical thermal model for the analysis of overhead conductor current-temperature relationship. Benchmark models using suggested guidelines (IEEE Standard 738-2006) is developed and the effect of various conductor parameters is analyzed. IEEE Standard 738-2006 is used to calculate solar heat gain values for radial temperature distribution calculation. This study also focuses on developing methods of tensile testing of composite cores. The tensile test data is analyzed to:

- Understand the fundamental tensile response of carbon composite core under uniaxial loading
- Estimate the tensile stiffness and strength
- Document the effect of temperature on failure stress.
- Compare the tensile properties at room and elevated temperatures
- Develop an ageing model based on the Weibull distribution.

1.2 Motivation and Background

Composite overhead conductors help to increase power delivery on existing right-of-ways (ROW) without violating the sag criterions. The need to transmit larger quantities of power through existing ROW's has led to increased interest in high temperature conductors. These conductors fall into a category known as high temperature, low sag (HTLS) conductors. Following are the different types presently in use:

1. ACSS (aluminum conductor steel supported) manufactured by the Southwire Company.
2. AAAC (all aluminum alloy conductor).
3. ACIR (aluminum conductor invar reinforced) manufactured by LS Cable.
4. Gap type conductor manufactured by J-Power.

Composite cores have higher strength and lower coefficients of thermal expansion when compared with the steel core used in traditional ACSR (aluminum conductor steel reinforced) or ACSS (aluminum conductor steel supported) conductors. With thermal line ratings dependent on the line clearance to ground (sag), these properties allow a significant rating increase over ACSR

or ACSS conductors. The published literature on these conductors indicates that they are stable in the range 150-200 °C, as compared to 100 °C for traditional ACSR conductors [1]. Published emergency ratings allow a conductor temperature of 240 °C [2].

The use of composite materials for the cores of overhead conductors is fairly recent. The selection of conductors is critical since wind, ice and tension loads that supporting structures must withstand are dependent on size/type of conductors used. Structure height is also largely dependent on the conductors selected since the maximum sag of phase conductors under maximum ice or maximum temperature conditions is governed by certain physical, mechanical and dimensional properties of the conductor.

Bare overhead conductors are usually classified as homogeneous or non-homogeneous. Homogeneous conductors are those in which the individual strands of wire comprising the cable are of the same material. Homogeneous conductors manufactured with relatively pure aluminum are called all-aluminum conductors (AAC); those manufactured with an aluminum alloy are called all-aluminum-alloy conductors (AAAC). Non-homogeneous conductors consist of a mixture of different wire materials. The most common type of bare overhead phase conductor is a non-homogeneous wire consisting of aluminum strands covering a steel core. This conductor is called aluminum conductor, steel-reinforced (ACSR). Non-homogeneous conductors possess properties that reflect the individual properties and relative percentages of the different materials forming the composite cable. Due to the stranding-induced helical form of the individual strands, both types of conductors exhibit lower composite rated breaking strength (4 to 11%), greater weight and higher electrical resistance per unit length of conductor (2 to 4%) than would be obtained if all the component strands were parallel.

Selection of the optimal conductor for a particular transmission or distribution line depends upon many factors, such as power requirement, pole structure, terrain, ambient conditions, costs of the conductor and supporting structures, and governmental and environmental constraints. In addition to the mechanical strength and electrical resistance of the conductor, pertinent properties of interest include the stress-strain relationship, thermal characteristics, and inductive and capacitive reactance.

There is a need to develop a confidence level with composite (polymeric) materials for them to be accepted as viable replacement of traditional overhead conductors employing a steel core. In this work an attempt has been made to add to the knowledge base for HTLS conductors by answering the following questions through this study:

- What are the thermal effects on the operating characteristics?
- What is the long term performance and expected life?
- How can we predict useful life and failure mechanisms?
- What measures can users employ to validate manufacturers' claims?

1.3 Previous Work

Presently, very little work has been published regarding the effect of temperature on tensile strength and radial temperature distribution in composite core conductors. The demand for electric power is still growing, but environmental restrictions, the time for construction and the cost of new overhead lines makes it essential to increase their transmission capacity as much as

possible. The maximum transmission capacity of long lines may depend on system stability, voltage drop or energy losses. The load capacity for shorter lines, including the majority of lines in North America and Europe, is limited by the maximum permissible temperature of the conductors, which determines the maximum sag and the long-term loss of strength of the conductors due to annealing [3].

Some early work on transmission line conductor thermal rating were conducted in France (Legrand, 1945) that realized the importance of transmission line conductor thermal rating. A steady state ampacity model based on the conductor heat balance equation was presented in 1956 by House and Tuttle. The IEEE and CIGRE offer standardized methods for the calculation of transmission line ampacity in the steady state, dynamic and transient states.

In a paper published by Douglas [4] on radial and axial temperature gradients in bare stranded conductor analyzes the temperature distribution within ACSR conductors. The analysis presented is based on experimental setup on ACSR conductor composed of a non-electrically conducting supporting core and an electrically conducting outer layer. Thus the core is isothermal and the temperature gradient occurs entirely in the conducting material of the outer layer. An effective thermal conductivity of the conducting layer has been used to obtain an expression for the temperature distribution. Douglas concludes that a significant temperature difference in the range of 15°C and 30°C can occur only under very high current conditions which are possible with dynamic ratings.

The Radial Conduction Model has been developed by Morgan and Findlay [5, 6]. This model calculates the radial temperature distribution within stranded conductors. Input variables for the model are the geometry, tension, layer currents, and yield stress of the nonferrous wires. Output variables are the radial forces, power loss and temperature of each layer, and the contact areas of the wires in adjacent layers.

The unified model developed by Gledja, Morgan and Findlay [3] includes the ferromagnetic power loss in the steel core and the redistribution of current due to the transformer effect. Input variables for this model are the geometry of the conductor, the electrical and magnetic properties of the ferrous and nonferrous materials, the total current and the temperature. Output variables are the complex layer currents, the power loss and the ac resistance.

The real time thermal model developed by Black and Rehberg [7] proposes a simplified transient ampacity model which predicts both the steady state and transient thermal behavior of conductors that are subjected to a step change in current. The simplified model provides results that are within 15 percent of a more complex, detailed transient ampacity model.

Morgan and Findley [6] predict that, with constant current, the radial temperature difference increases as the axial tension and the air pressure decreases. To validate these predictions, a length of 91/4.04 mm AAC conductor was tensioned within a vacuum chamber and the temperature of each layer of wires was measured for various total currents. It was found that the radial temperature difference increased with increasing resistive power loss per unit length, with decreasing axial tension and air pressure. They also found that the effective radial thermal

conductivity is independent of the power loss, and increases with increasing axial tension and air pressure.

The thermal conductivity of the composite stranded conductor is much less than the thermal conductivity of the solid component metals [5]. The conductor is composed of individual strands of material which, although tightly wound, are not in total thermal contact with each other. Figure 1.1 shows a typical aluminum conductor steel reinforced (ACSR) conductor. The air between the conductor strands acts as an insulating material which impedes the conduction of heat to the outer surface of the conductor. This significant resistance to the radial heat transfer can produce a radial temperature gradient within the conductor.

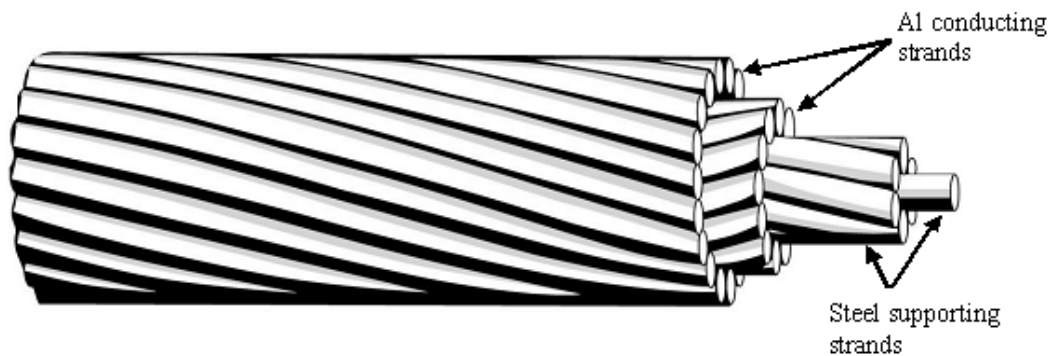


Figure 1.1: Typical ACSR conductor
(Inspired by Southwire Company)

The current in ampere that a conductor can carry for a given ambient temperature is referred to as the ampacity of the conductor. All conductors have a static ampacity rating. This is the ampacity value when there is no wind. The static ampacity value may be selected to be a conservative value to minimize the effects of thermal creep and loss of strength in the conductor as well as preventing excessive conductor sag. When the current loads are maintained below the static rating, the conductor remains fairly isothermal. Conductors also have dynamic ampacity values which allow for an upper current load limit which is dependent on the wind velocity. Significantly higher ampacity values compared to static values are possible under high wind conditions. Dynamic ampacity ratings can be as high as 200% above the static rating of a conductor. Under these higher loads, the temperature difference between the core of the conductor and the outer surface has been reported to be as large as 15°C to 30°C [8].

This significant temperature difference should be taken into account when computing conductor sag which is dependent on the temperature distribution in the conductor. Under extreme conditions, the knowledge of the size of the temperature gradient should be used in determining any thermal creep and loss of strength in the conductor.

1.4 Thermal Rating of Bare Overhead Conductors

The maximum continuous current carrying capacity of a conductor, called the maximum thermal rating, is one of the major factors considered when selecting a conductor for an overhead transmission line. The thermal rating is a function of local weather conditions, conductor characteristics and the maximum design operating temperature of the conductor. The major

consideration involving the determination of the thermal rating, or ampacity, of an overhead transmission conductor is the effect of the conductor heating on sag and long term loss of strength. Because conductor temperature indirectly determines allowable conductor current, the factors affecting the actual conductor temperature must be considered. The maximum allowable continuous current that corresponds to the maximum allowable conductor temperature is called the steady-state thermal rating of the line. The method used to calculate this rating assumes the conductor is in thermal equilibrium at the maximum allowable conductor temperature. If the values of ambient conditions and conductor variables are known, the ampacity can be calculated using the steady-state heat balance equation. In determining steady-state ratings, a continuous current is calculated that would yield the maximum allowable conductor temperature for certain weather assumptions and conductor parameters. Conservative weather conditions of low wind speed (2 to 3 ft/sec perpendicular to the conductor) and high ambient temperature (35 °C to 40 °C) are normally used to calculate heat loss rates.

The “IEEE Standard 738-2006 titled *method for calculation of bare overhead conductor temperatures and ampacities under steady-state conditions*” [9], is discussed in Chapter 3 and a MATLAB program based on this standard is presented in Appendix A. The method from IEEE Standard 738-2006 has been used to calculate the ampacities of conductors for an ambient temperature of 25 °C, a conductor temperature of 180 °C and a 2 ft/s wind that is exposed to sunlight. An average value of 0.5 has been used for the emissivity and absorptivity.

1.5 Organization of the Report

Chapter 2 reviews the thermal ageing of composite conductors. An effect of high temperature on metal matrix cores and carbon composite cores and thermal characteristics through experiments conducted in laboratory are also discussed. In Chapter 3, the IEEE Standard 738-2006 is discussed for steady state conditions. The effect of various parameters on the current-temperature relationship is also established. In Chapter 4, theoretical simulations of radial temperature distribution in composite overhead conductor are discussed. The effect of conductor current, ambient temperature, emissivity and absorptivity on radial temperature of conductors are discussed. Chapter 5 gives a detailed analysis of mechanical characteristics of composite cores through experimental observations and theoretical analysis. It also includes tensile test as a function of temperature, discusses design of tensile test grips and the use of Weibull statistics for ageing analysis. Chapter 6 presents the conclusions, recommendations and future work regarding this project.

2. Thermal Ageing of Composite Conductors

2.1 Introduction

Composite cores have higher mechanical strength and lower coefficients of thermal expansion when compared with the steel core used in traditional ACSR (aluminum conductor steel reinforced) or ACSS (aluminum conductor steel supported) conductors. With line ratings (current carrying capacity at maximum operating temperature) dependent on the line clearance to ground (sag), these properties allow for a significant rating increase over ACSR or ACSS conductors. The short term and long term exposure of composite core to high temperatures is a primary concern for acceptance of this new type of overhead conductors. There is a concern about potential loss of mechanical strength due to fiber matrix degradation. It is important to assess what factors can weaken mechanical strength and quantify the reduction. Also needed is an understanding of the mechanisms responsible for changes in the mechanical strength and determine if these can be addressed satisfactorily, because users expect overhead conductors to last indefinitely (at least 100 years) [10].

2.2 Composite Conductors

Metal matrix composite conductor is a non-homogeneous conductor consisting of high-temperature aluminum zirconium strands covering a stranded core of fiber reinforced composite wires. The ACCR core consists of Al_2O_3 fibers, about $10\ \mu\text{m}$ in diameter, in metallic matrix (aluminum) alumina fibers in an aluminum matrix. There is no dielectric barrier in the ACCR core. Therefore the ACCR core will carry some current, although a majority of it will flow in the aluminum conductors owing to the skin effect.

Carbon composite conductor incorporates a lightweight advanced core made of continuous glass and carbon fibers with polymer resin over which a trapezoidal shaped aluminum wires are wrapped. The ACCC core evaluated consists of carbon fibers surrounded by a sheath of glass fibers all bonded with an organic epoxy resin. The fiberglass sheath serves as a barrier and prevents corrosion by separating two dissimilar materials (carbon and aluminum).

The fundamental difference in these conductors is the construction of the core. Both the composite core and the outer aluminum-zirconium (Al-Zr) strands contribute to the overall conductor strength. Each core wire contains thousands of high strength micrometer sized fibers. The fibers are continuous, oriented in the direction of the wire. Both the carbon composite conductor and the aluminum metal matrix conductor are dramatically superior to the conventional ACSR conductors of comparable diameter. Both cores employ either circular or trapezoidal aluminum conductors as shown in Figure 2.1 and Figure 2.2.



Figure 2.1: Aluminum conductor composite reinforced (ACCR)



Figure 2.2: Aluminum conductor carbon composite (ACCC)

The primary role of the conductor core is to provide mechanical strength, but it may degrade due to aging. It is well known that organic materials are more susceptible to aging than inorganic materials [10]. The nature of construction of both types of composite cores gives rise to interfaces, both microscopic and macroscopic. The microscopic interfaces in the ACCR conductor core are between each alumina ceramic fiber and the aluminum matrix, and in the ACCC conductor core are between each fiberglass and carbon fiber with epoxy resin. The interface between the core and aluminum strands constitutes a macroscopic interface for both types of composite conductors. The ACCC conductor core has an additional macroscopic interface between the fiberglass sheath and carbon fibers, within the epoxy resin.

2.3 Thermal Stress of the Carbon Composite Core

Carbon composite cores were subjected to thermal stress. To this end, the carbon composite cores were cut into 10 samples of 1 inch length. Out of the 10 samples, five samples were heated in a furnace at 175 °C and the other five samples at 200 °C. A virgin unheated sample was used as the control reference for the experiments. Figure 2.3 shows the cross-section of the control sample.



Figure 2.3: The cross-section of a new carbon composite core sample

Heated samples were removed from the furnace every 5 days to check the degradation of the sample. The degradation of the sample was checked by keeping the sample in contact with high temperature, so as to check the worst conditions of the sample and making the conditions similar to those in service for a very long time (120 hrs) under normal conditions. The Figure 2.4 shows the degradation of the sample by cracking of the cross-section of the sample.



Figure 2.4: The cross-section of the sample kept in furnace for 5 days at 175 °C

The sample in Figure 2.4 was kept in the furnace for 5 days (4 hrs/day) at 175 °C, after which physical changes were observed. The cross-section of the sample was cracked axially from one end of the surface to the other. Figure 2.5 shows the cross section of another same sample after 15 days in the oven at 200 °C.



Figure 2.5: The cross-section of the sample kept in furnace for 15 days at 200 °C

The figure shows the clear degradation of the carbon composite core sample. All the samples which were kept in the oven for 120 hrs had been cracked to some extent and the depth of the crack was approximately a few nano-meters.

The crack of the sample can be explained by the expansion of the glass carbon fibers in the carbon core. When the sample was kept in the furnace, the carbon fibers in the core expand accordingly to the temperature increase and due to the expansion of the carbon fibers; the fibers crack down as they do not have the much needed space to expand inside the core. Therefore, the crack varies from the sample to sample and also varies with time. Figure 2.6 shows degradation of fiberglass sheath after exposing to temperature of 200 °C for 10 days.



Figure 2.6: An aged sample showing the polymer resin of the carbon composite core

The above figures compare the polymer resin of the carbon composite core. It can be observed that the surface of the material is highly degraded and the color of the sample has changed darker. The maximum temperature the carbon composite core can withstand without damage is 225 °C. To check the worst conditions, the aged sample was kept at 200 °C but the sample could not withstand the high temperature and it was cracked and degraded at a very high extent.

2.4 Experimental Results for Metal Matrix and Carbon Composite Core

Figure 2.7 shows scanning electron microscopic (SEM) images of metal matrix core subjected to a temperature of 210°C for 120 hrs and virgin sample. There were no significant changes observed.

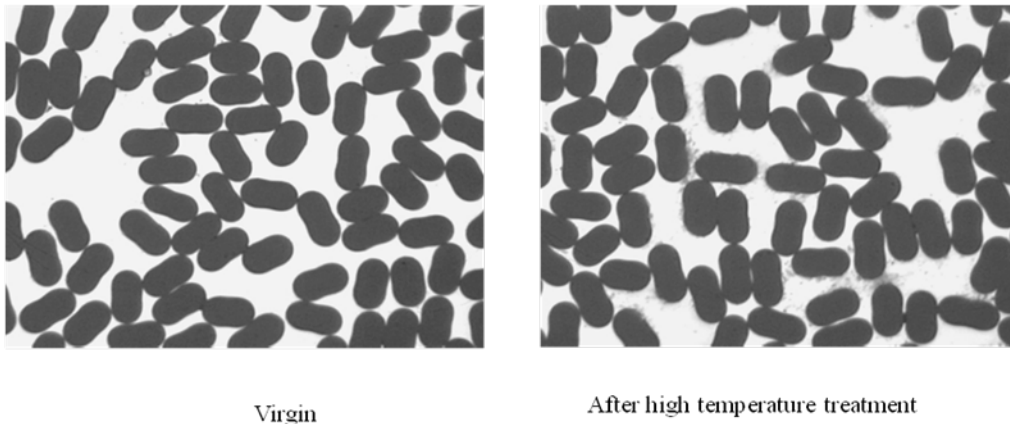


Figure 2.7: SEM image of a metal matrix core subjected to 210 °C for 120 hrs and virgin sample

Figure 2.8 shows the scanning electron microscopic image of carbon composite core subjected to a temperature of 210°C for 120 hrs and virgin sample.

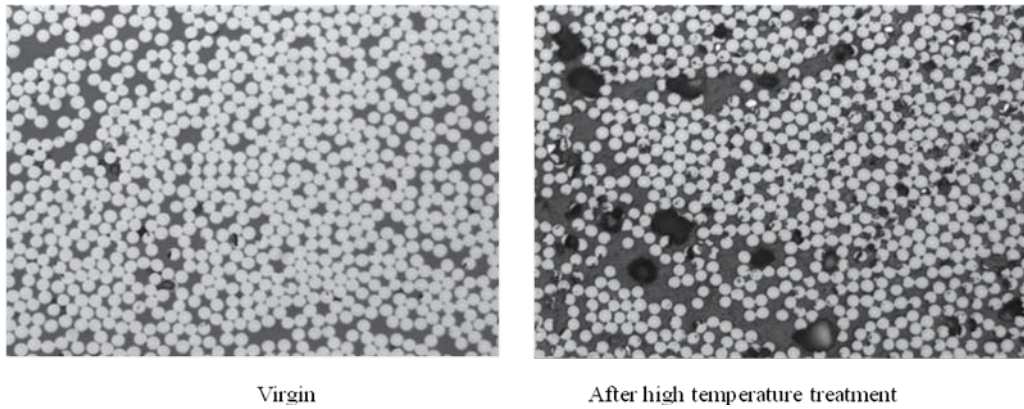


Figure 2.8: SEM image of a carbon composite core subjected to 210 °C for 120 hrs and virgin sample

Some changes were seen in terms of void growth in matrix of carbon fibers when subjected to 210 °C for 120 hrs. Figure 2.9 shows the change in microstructure due to thermal stress in carbon composite core.

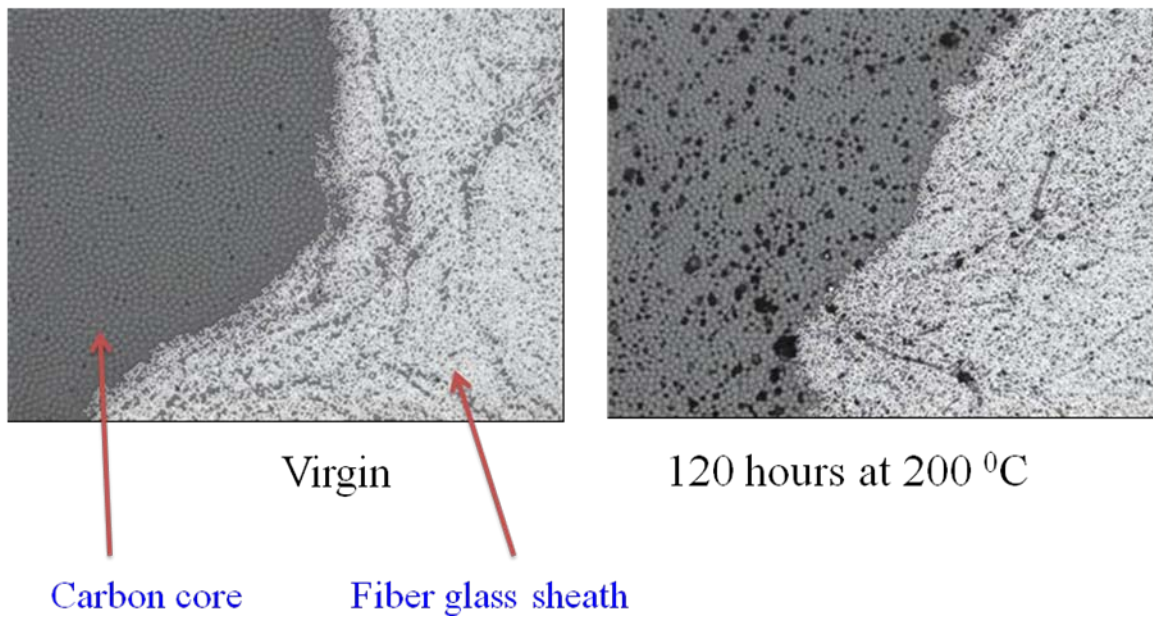


Figure 2.9: SEM image of a carbon composite core subjected to 210 °C for 120 hrs and virgin sample

Figure 2.10 shows cracking in a resin of carbon composite core when subjected to 240 °C for 120 hrs.

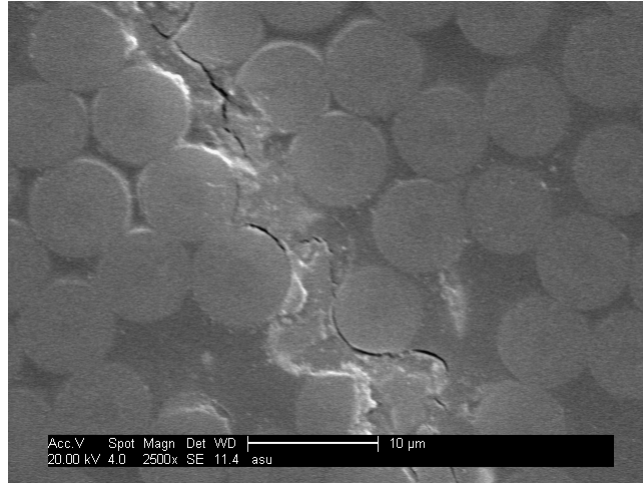


Figure 2.10: Cracking in resin of carbon composite when subjected to 240 °C for 120 hrs.

It is important to assess what factors can weaken mechanical strength, quantify the reduction, understand the mechanisms and determine if these can be addressed satisfactorily.

3. Calculating the Current-Temperature of Bare Overhead Conductors

3.1 Introduction

Temperature is a factor that affects many conductor characteristics, such as thermal expansion and conductivity. Consequently, temperature must be considered in the determination of conductor thermal ratings. Regardless of climatic conditions, overhead lines must deliver power with maximum efficiency. The continuous current carrying capacity of overhead lines must be determined for varying weather and loading conditions based on a designated maximum temperature. This maximum allowable temperature is specified:

- 1) To limit the reduction of conductor tensile strength due to annealing to 10% or less over the life of the line and
- 2) To prevent conductor sag due to thermal elongation from violating predetermined ground clearances.

The maximum allowable conductor temperature applies to both steady-state thermal ratings and transient (emergency) thermal ratings. In determining steady-state ratings, a continuous current is calculated that would yield the maximum allowable conductor temperature for certain weather assumptions and conductor parameters. Typical, conservative, weather assumptions used in steady-state ratings allow for considerable increases in current under emergency conditions.

Because conductor temperature indirectly determines allowable conductor current, the factors that determine it must be studied. Conductor temperature is a function of the heat produced from the current flowing through the conductor, the thermal properties of the conductor, and the surrounding ambient conditions. The conductor temperature is raised primarily through heat input from ohmic losses (I^2R), and partially from solar radiation. Ohmic losses are a function of conductor resistance and current; solar radiation input is dependent on the conductor's absorptivity. The conductor temperature is also affected by the cooling caused by heat loss through convection and conductor radiation. Convection, the major source of heat loss, is a function of the air temperature, and wind speed and direction. Conductor radiation, having a lesser effect on conductor temperature, is affected by air temperature and the conductor's emissivity.

3.2 Steady-State Heat Balance

In steady state, heat input to the bare overhead conductor from solar radiation and ohmic (I^2R) losses balances the heat lost by convection and radiation cooling. For a unit length of bare overhead conductor, the steady-state heat balance equation is:

$$q_c + q_r = q_s + I^2 R_{Tc} \quad (3.1)$$

solving for I ,

$$I = \sqrt{\frac{q_c + q_r - q_s}{R_{Tc}}} \quad (3.2)$$

where:

q_c = convection heat loss, w/ft

q_r = radiated heat loss, w/ft

q_s = heat gain from sun, w/ft

R_{Tc} = 60 Hz ac resistance of conductor at operating temperature T_c , Ω/ft .

Solar Heat Gain: Solar heating normally raises the conductor temperature by 5 °C to 10 °C above the air temperature, and is usually included in thermal rating calculations. The solar heat gain equation is:

$$q_s = \alpha * Q_s * \sin(\theta) * A' \quad (3.3)$$

where:

Q_s = total solar and sky radiated heat flux, W/ft^2

θ = effective angle of incidence of the sun's rays, *degrees*

A' = projected area of conductor, *square feet per linear foot*

The effective angle of incidence, θ , of the sun's rays is calculated as follows:

$$\theta = \cos^{-1}[\cos(H_c)\cos(Z_c - Z_l)] \quad (3.4)$$

where:

H_c = altitude of sun, *degrees*

Z_c = azimuth of sun, *degrees*

Z_l = azimuth of line, *degrees*.

An average value of the absorptivity of 0.5 is often used when actual conductor surface condition is unknown. The normal solar heat flux, Q_s , at ground level varies with latitude, reaching a maximum of nearly 100 W/ft^2 in the summer in the U.S.A. Values of the solar altitude, H_c , and azimuth of the sun, Z_c , are taken from Reference [9]. The azimuth of power lines, Z_l , is assumed to be 0° (or 180°) for North-South lines and 90° (or 270°) for East-West lines.

Convection Heat Loss: The major heat loss of an overhead conductor occurs through convection and is typically three to four times as large as the radiated heat loss. Forced convection heat loss occurs in non-still air and is proportional to the conductor temperature differential with the air temperature, conductor diameter, and wind speed. In still air, natural convection occurs and is equivalent to forced convection with a wind speed of approximately 0.5 ft/s .

Forced Convection Heat Loss: In an attempt to find an accurate model of convection heat loss over the whole range of possible wind speeds, forced convection heat loss is represented by two separate calculations:

$$q_{c1} = \left[1.01 + 0.371 \left(\frac{D\rho_f V_w}{\mu_f} \right)^{0.52} \right] k_f (T_c - T_a) \quad (3.5)$$

and

$$q_{c2} = 0.1695 \left(\frac{D\rho_f V_w}{\mu_f} \right)^{0.6} k_f (T_c - T_a) \quad (3.6)$$

where:

q_c = convection heat loss, W/ft

μ_f = absolute viscosity of air temperature T_f , $lbs/ft-hr$

ρ_f = density of air temperature T_f , W/ft^3

D = conductor diameter, *in*

V_w = wind speed, *ft/hr*
 T_c = conductor temperature, $^{\circ}C$
 T_a = ambient temperature, $^{\circ}C$.

$$T_f = \left(\frac{T_c + T_a}{2} \right) \quad (3.7)$$

The first equation, q_{c1} , applies at low winds, but gives convective heat losses that are too low at high speeds. The second equation, q_{c2} , applies at high wind speeds and predicts heat losses that are too low at low wind speeds. At any wind speed, convective heat loss is calculated using both equations. The larger of the two is conservatively chosen for thermal rating calculations. If the wind is not perpendicular to the conductor, then the convective cooling term is multiplied by the wind direction factor, K_{angle} , as defined below.

$$K_{angle} = 1.194 - \cos(\phi) + 0.194 \cos(2\phi) + 0.368 \sin(2\phi) \quad (3.8)$$

where:

Φ = angle between wind and axis of the conductor, *degrees*.

Use of this equation suggests wind blowing parallel to a line can result in approximately 60% lower convective heat loss than a wind of the same speed blowing perpendicular to the line.

Natural Convection Heat Loss: With zero wind speed, the forced convection goes to zero, but natural convection due to rising hot air still occurs. The natural convection heat loss can be calculated by:

$$q_c = 0.283 \rho_f^{0.5} D^{0.75} (T_c - T_a)^{1.25} \quad (3.9)$$

where:

ρ_f = density of air, *lbs/ft³*
 D = conductor diameter, *in*.

The conservative IEEE method [9] uses the larger of the forced and natural convection heat losses at low wind speeds. The computer program developed in MATLAB also implements this approach. The values of air density, air viscosity, and the coefficient of thermal conductivity of air, are taken from [9].

Radiation Heat Loss: The radiated heat loss per unit length of conductor is approximately equal to the convective heat loss under still air conditions and is negligible at wind speeds above 10 *mph*. The radiated heat loss is dependent upon the conductor diameter, emissivity and conductor temperature rise above ambient and can be determined by using the following equation:

$$q_r = 0.138 D \varepsilon \left[\left(\frac{K_c}{100} \right)^4 - \left(\frac{K_a}{100} \right)^4 \right] \quad (3.10)$$

where:

q_r = radiated heat loss, *W/ft*
 ε = emissivity
 D = diameter of conductor, *in*
 K_c = temperature of conductor, $^{\circ}K$
 K_a = ambient temperature, $^{\circ}K$.

Emissivity value of 0.5 has been used in the computer program since actual conductor surface condition is unknown.

Conductor Ohmic Loss: The ohmic, or I^2R , loss per unit length of conductor is equal to the conductor resistance in ohms per unit length times the square of the *rms* electrical current in amperes. The 60 Hz ac resistance of a bare, stranded conductor varies with metal conductivity, frequency, average current density, and temperature. To determine thermal ratings at temperature for which no resistance values are listed, the resistance at the desired temperature may be calculated with the following linear equation:

$$R_{TC} = R_{TL} + \left[\frac{R_{TH} - R_{TL}}{T_H - T_L} \right] (T_C - T_L) \quad (3.11)$$

where:

R_{TC} = resistance calculated at temperature T_C , Ω

R_{TL} = 60 Hz ac resistance at temperature T_L , Ω

R_{TH} = 60 Hz ac resistance at temperature T_H , Ω

T_L = conductor temperature at which the resistance R_{TL} is specified, $^{\circ}C$

T_H = conductor temperature at which the resistance R_{TH} is specified, $^{\circ}C$

T_C = conductor temperature at which new 60 Hz resistance is desired, $^{\circ}C$.

Skin Effect: The skin effect is present for a conductor carrying alternating current and is a function of the internal flux in a conductor. Alternating current tends to flow near the outside of a conductor, yielding higher current density on the outer layers and increasing the effective resistance. If the conductor is made from or contains a ferromagnetic material, such as steel, the skin effect is increased. For a stranded conductor consisting entirely of aluminum or copper, experimental studies by Kennelly, et al [11], indicate that skin effect in concentric-lay-stranded conductor is identical to that of a solid cylindrical conductor having the same dc resistance. The skin effect is not directly dependent on the magnitude of the current in the conductor [12].

3.3 Computer Program for Thermal Rating

The computer program developed in MATLAB (Appendix A) to calculate the thermal rating (ampacity) of conductors is based on the IEEE Standard 738 [9]. The computer program can be used to calculate:

1. Steady-state thermal rating: ratings can be calculated, given a maximum allowable conductor temperature, weather conditions, and conductor characteristics.
2. Steady-state conductor temperature: can be determined for a given electrical current, given the weather conditions, and conductor characteristics.

IEEE 738 Steady State Current-Temperature Relationship

The IEEE 738 standard was studied for steady state current temperature relationship of bare overhead ACSR conductor and a program was written in MATLAB based on the methods presented herein. The results for various conditions are shown in following section. Case 1 in Table 2 is considered as a standard condition. Input parameter variations upon this standard condition are highlighted with table cell shading, and were changed for while keeping the other

input parameters constant. The output parameters are summarized in Table 3.4 for the cases presented in Table 3.1 and Table 3.3.

Table 3.1: Case description for Table 3.2

Case description
1* Standard results for ACSR conductor
2* Changing the heat capacity of conductor (mCp) - using the values of ACCC 1020 kcmil / Drake conductor with same conditions as case 1
3* ACCC 2727 kcmil / Bluebird conductor with other conditions kept as for case 2
4* Change in Sun time, other conditions same as case 3
5* Change in Sun time, other conditions same as case 3

Table 3.2: Inputs for conductor temperature (IEEE Standard 738-2006)

Input Parameters	Case Numbers				
	1	2	3	4	5
Solar Hour (Sun time), Hr	14	14	14	12	18
Conductor Latitude in Deg (CDRLATDEG), °C	43	43	43	43	43
Day of the year (NDAY), Day	161	161	161	161	161
Coefficient of Absorption (ABSORP)	0.5	0.5	0.5	0.5	0.5
Air Clarity Clear(0); Industrial(1) (A3)	0	0	0	0	0
Angle between wind and conductor axis in Deg (Z1DEG), °C	90	90	90	90	90
Conductor Diameter (D), mm	28.12	28.12	44.75	44.75	44.75
Ambient Temperature (TAMB), °C	40	40	40	40	40
Emissivity (EMIV)	0.5	0.5	0.5	0.5	0.5
Velocity of wind (VWIND), m/s	0.61	0.61	0.61	0.61	0.61
Conductor Elevation (CDRELEV)	0	0	0	0	0
AC Resistance at 75 °C (RHI), Ω/m	8.69E-05	6.75E-05	2.83E-05	2.83E-05	2.83E-05
AC Resistance at 25 °C (RLO), Ω/m	7.28E-05	5.64E-05	2.46E-05	2.46E-05	2.46E-05
Heat capacity of conductor (mCp), W/s	1066+24 3	756	2040.8	2040.8	2040.8

Table 3.3: Case description for Table 3.4

Case description
6* Change in day of the year only, other conditions same as case 3
7* Change in day of the year only, other conditions same as case 3
8* Change in wind velocity only, other conditions same as case 3
9* Change in wind velocity only, other conditions same as case 4

Table 3.4: Inputs for conductor temperature (IEEE Standard 738-2006)

Input Parameters	Case Numbers			
	6	7	8	9
Solar Hour (Sun time), Hr	14	14	14	14
Conductor Latitude in Deg (CDRLATDEG), °C	43	43	43	43
Day of the year (NDAY), Day	250	365	161	161
Coefficient of Absorption (ABSORP)	0.5	0.5	0.5	0.5
Air Clarity Clear(0); Industrial(1) (A3)	0	0	0	0
Angle between wind and conductor axis in Deg (Z1DEG), °C	90	90	90	90
Conductor Diameter (D), mm	44.75	44.75	44.75	44.75
Ambient Temperature (TAMB), °C	40	40	40	40
Emissivity (EMIV)	0.5	0.5	0.5	0.5
Velocity of wind (VWIND), m/s	0.61	0.61	1	0
Conductor Elevation (CDRELEV)	0	0	0	0
AC Resistance at 75 °C (RHI), Ω/m	2.83E-05	2.83E-05	2.83E-05	2.83E-05
AC Resistance at 25 °C (RLO), Ω/m	2.46E-05	2.46E-05	2.46E-05	2.46E-05
Heat capacity of conductor (mCp), W/s	2040.8	2040.8	2040.8	2040.8

Table 3.5: Results for conductor temperature (IEEE Standard 738-2006)

Output Parameters	Case Numbers				
	1	2	3	4	5
Solar Gain (QS), W/m	12.430 3	12.430 3	19.781 6	22.857 2	5.1991
Radiation heat loss (QR), W/m	24.363 1	18.083 6	11.132 7	11.944 1	7.3863
Convection heat loss (Qcfinal), W/m	81.939 5	64.543 4	35.887 2	38.252 2	24.568 7
(Rtc), Ohm/m	9.39E-05	7.02E-05	2.72E-05	2.73E-05	2.68E-05
Steady state conductor current rating (Is), A	1000	1000	1000	1000	1000
Conductor temperature rating (TCDR), °C	100.0	87.1	60.7	62.0	54.1

Table 3.6: Results for conductor temperature (IEEE Standard 738-2006)

Output Parameters	Case Numbers			
	6	7	8	9
Solar Gain (QS), W/m	0.3545	13.0938	19.7816	19.7816
Radiation heat loss (QR), W/m	10.7129	9.3938	5.8645	13.3384
Convection heat loss (Qcfinal), W/m	34.6521	30.718	40.4684	33.9529
(Rtc), Ohm/m	2.72E-05	2.70E+00	2.66E-05	2.75E-05
Steady state conductor current rating (Is), A	1000	1000	1000	1000
Conductor temperature rating (TCDR), °C	59.9	57.7	51.3702	64.3

Table 3.6 is summarized based on case descriptions in Table 3.1 and Table 3.3.

3.4 Results

Figure 3.1 shows plot of conductor temperature vs. time for conductor current rating of 1000 A.

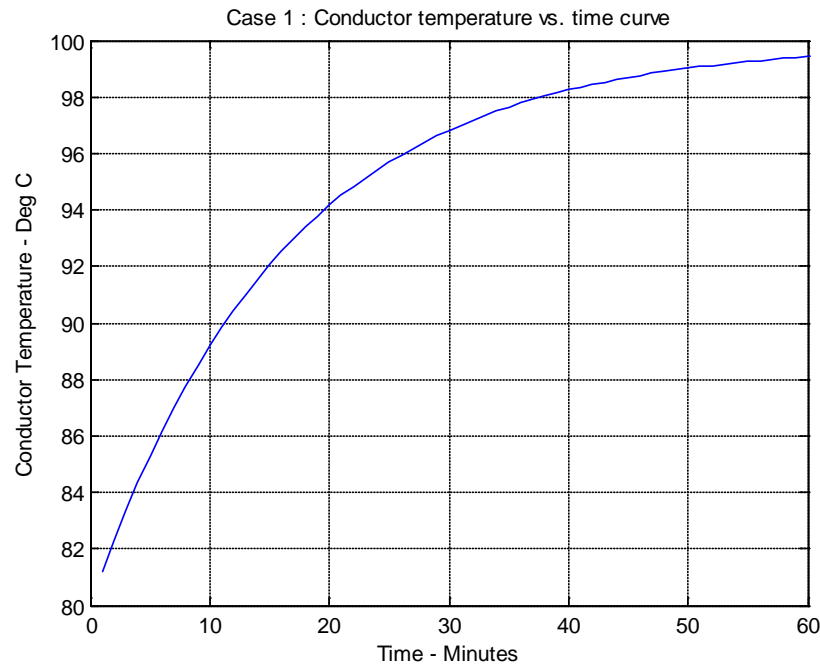


Figure 3.1: Conductor temperature vs. time curve for base case 1.

Figure 3.1 is treated as standard curve for comparison with different cases mentioned in Table 3.1 and Table 3.3. Various parameters were changed and their effect on conductor temperature was studied. Figure 3.2 shows the result for case 3, where diameter of conductor was changed from 28.12 mm to 44.75. It shows that there is a reduction in temperature compared to standard case shown in Figure 3.1. In case 4, Sun time is changed from 14 hr to 12 hr and Figure 3.3 shows that there is a decrease in conductor temperature. Figure 3.4 shows further reduction in conductor temperature if Sun time is changed from 12 hr to 18 hr. Case 6 and 7 shows an effect of day of the year on conductor temperature. The plots for case 6 and 7 are shown in Figure 3.5 and Figure 3.6. The effect of wind velocity is shown in Figure 3.7 and Figure 3.8.

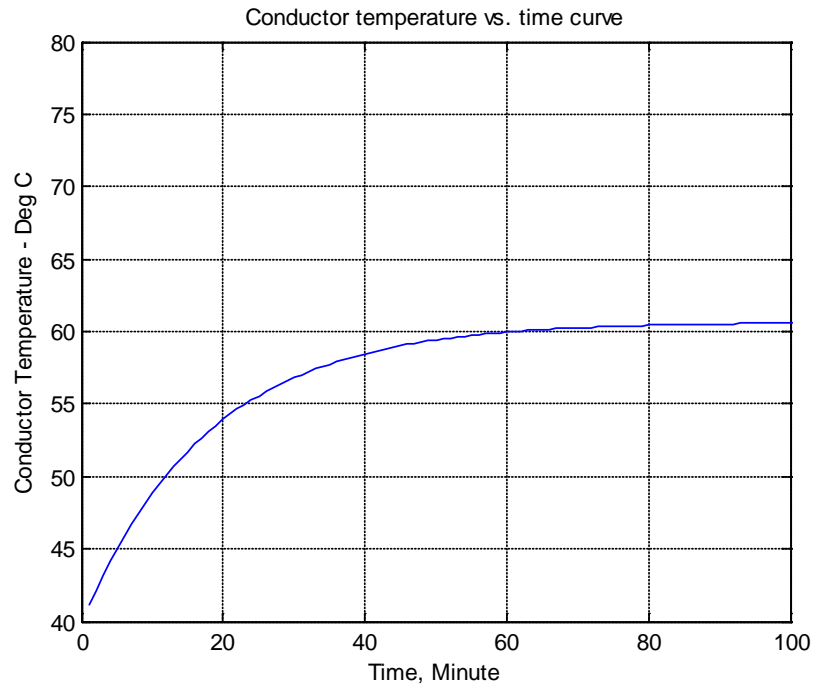


Figure 3.2: Conductor temperature vs. time curve for case 3 (change in ac resistance & heat capacity).

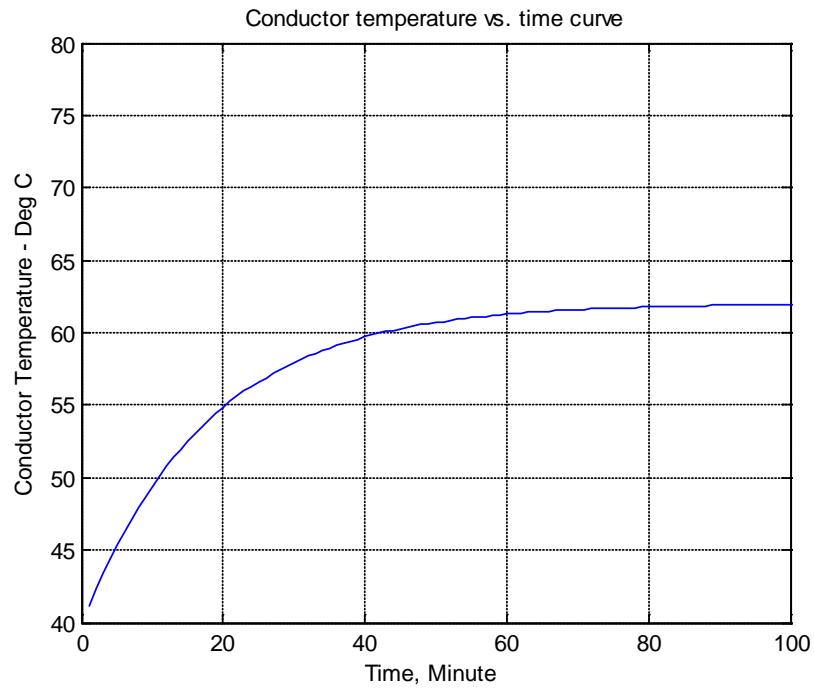


Figure 3.3: Temperature vs. time curve for case 4 (change in sun time 12 hr)

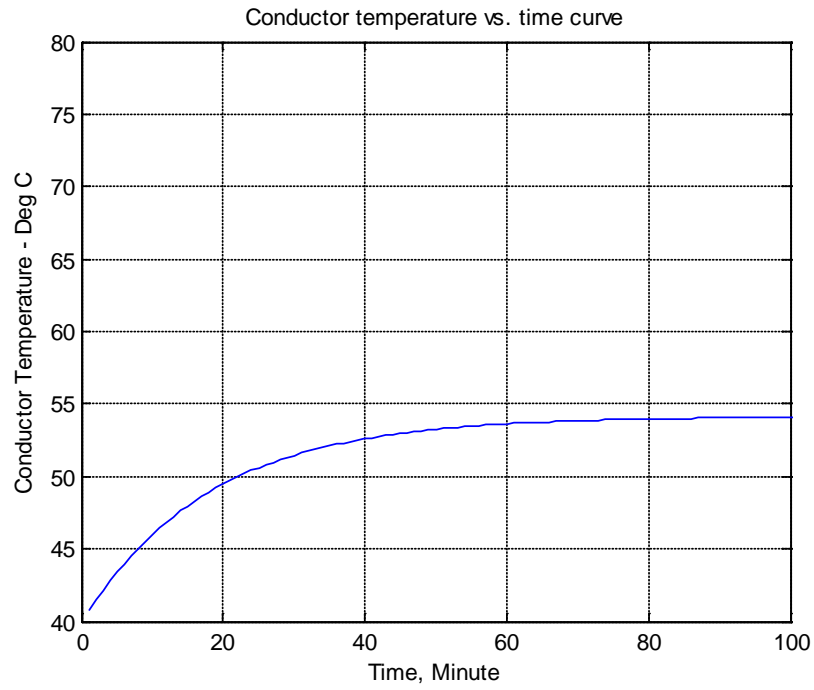


Figure 3.4: Temperature vs. time curve for case 5 (change in sun time 18hr)

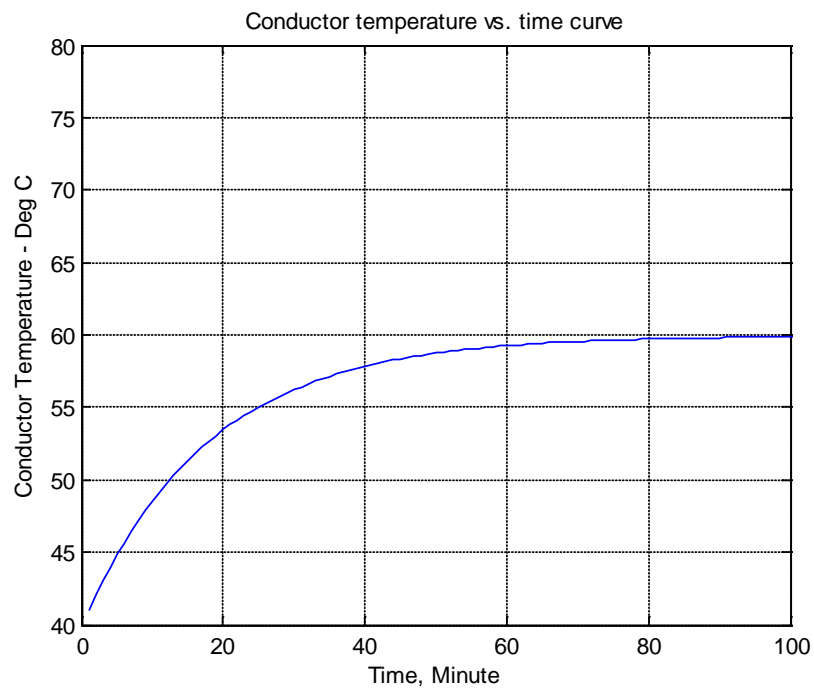


Figure 3.5: Temperature vs. time curve for case 6 (change in day of the year, NDAY=250)

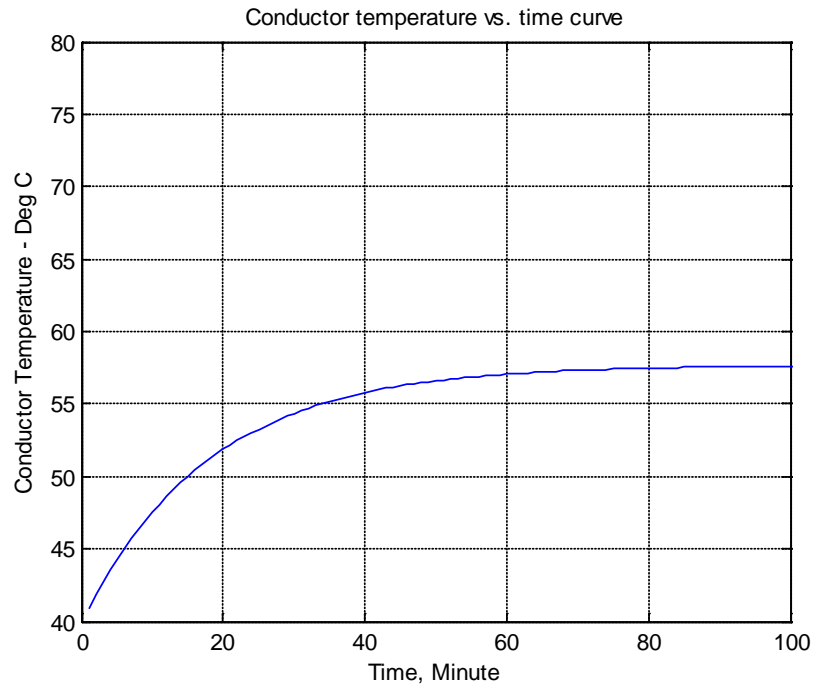


Figure 3.6: Temperature vs. time curve for case 7 (change in day of the year, NDAY=365)

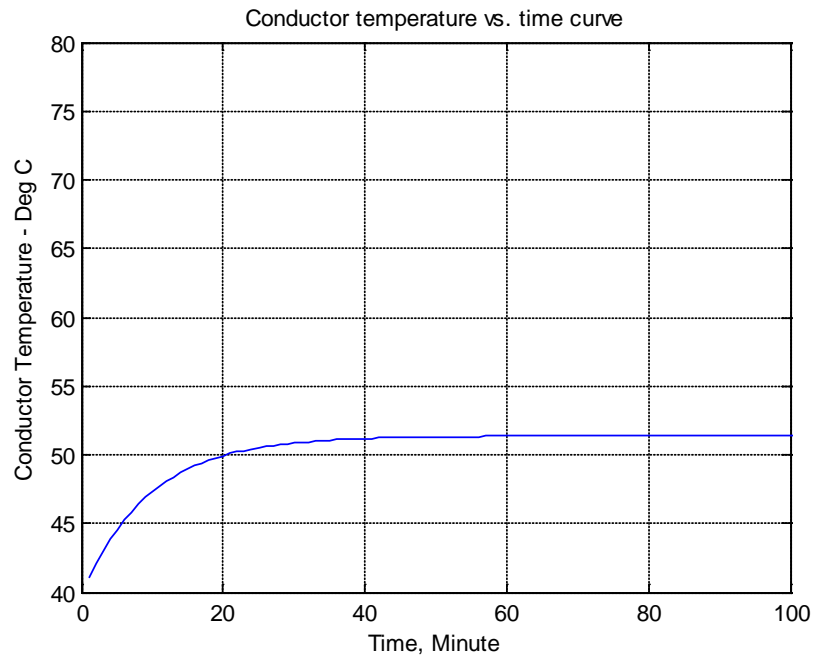


Figure 3.7: Temperature vs. time curve for case 8 (change in velocity of wind, 1 m/s)

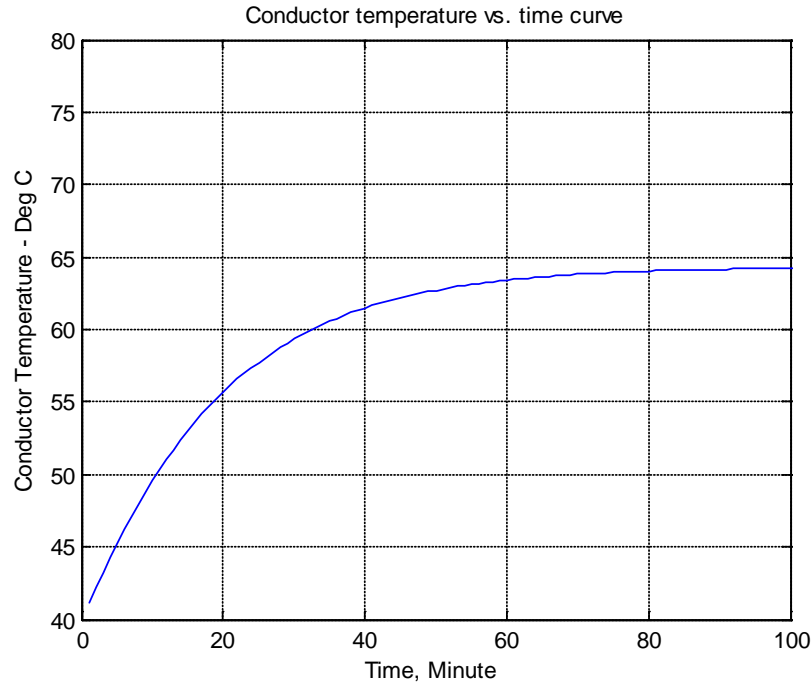


Figure 3.8: Temperature vs. time curve for case 9 (change in velocity of wind, 0 m/s)

3.5 Conclusion

The effect of various conductor parameters was studied for the current-temperature relationship. The steady-state temperature is dependent on the thermal properties of the entire conductor. Under short-circuit conditions, due to the momentary nature of the current surge, the core does not play a role and the temperature is determined by the aluminum strands. The standards permit short term (0.05-0.33 s) rise in temperature in the 180-340 °C range. For ACSR there is an upper limit of 645 °C at which the aluminum starts to melt, but the mechanical strength is retained due to the steel core.

4. Radial Temperature Distribution in Composite Conductors

4.1 Introduction

An attempt is made to create a mathematical model for the radial temperature gradients within bare overhead composite core conductors. The radial temperature of the conductor is derived from the general heat equation as well heat transfer to the outside. The differential equations were derived, which assures conservation of energy within conductor to obtain a temperature variation expression. Previously published mathematical models were used for verification of results on ACSR conductors. After validation of the model, an analysis was done to develop current-temperature relationship for aluminum conductor carbon composite (ACCC) overhead conductors. The radial temperature gradient is particularly important for high ampacity transmission line conductors since they are capable of operating at high temperatures.

4.2 Conduction Equation for Overhead Conductor

The following assumptions were considered for the conduction equation:

1. The conductor current is steady
2. There is constant heat generation per unit volume
3. The temperature of the conductor is only a function of the radial position
4. Thermal conductivities of the materials are constant
5. The conductor electrical resistance varies linearly with temperature
6. The radiation from the conductor takes place to surroundings at the temperature of the ambient air.

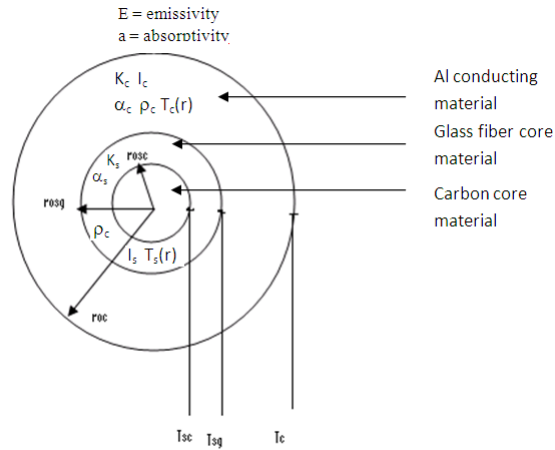


Figure 4.1: Typical composite conductor

Basically, there are two types of materials in the conductor: the conductor layers itself and the core. The core is further divided into the carbon composite material and a glass fiber layer. Both materials have different conducting properties. The carbon composite core is a semiconducting material whereas glass fiber is an insulating material. The results of ACSR conductors are compared with those of ACCC. The comparison is made with the results published in reference paper [13] for ACSR.

The radial temperature of the conductor is derived from the general heat equation. The general conduction equation for a transmission line conductor in terms of the Laplacian form [14] is

$$\nabla^2 T + \frac{q}{k} = \frac{1}{\alpha} \frac{\partial T}{\partial t} \quad (4.1)$$

$$\frac{1}{r} \frac{\partial}{\partial r} \left(r \frac{\partial T}{\partial r} \right) + \frac{1}{r^2} \frac{\partial^2 T}{\partial \Phi^2} + \frac{\partial^2 T}{\partial z^2} + \frac{q}{k} = \frac{1}{\alpha} \frac{\partial T}{\partial t} \quad (4.2)$$

In a one-dimensional cylindrical conductor, the conduction equation becomes,

$$\frac{1}{r} \frac{\partial}{\partial r} \left(r \frac{\partial T}{\partial r} \right) + \frac{q}{k} = \frac{1}{\alpha} \frac{\partial T}{\partial t} \quad (4.3)$$

If the temperature is steady and a function of only the radial coordinate, the conduction equation becomes

$$\frac{1}{r} \frac{d}{dr} \left(r \frac{\partial T}{\partial r} \right) + \frac{q}{k} = 0 \quad (4.4)$$

The generation term q in a conduction equation is due to electric heating which is a result of $I^2 R$ losses.

$$q = \frac{I^2 R}{A} \quad (4.5)$$

where:

A = conductor cross sectional area, m^2

R = resistance per unit length, Ω

I = Total current flowing through conductor, A.

Let,

I_t = total current through composite conductor, A

I_c = current flowing through conductor strands, A

I_s = current flowing through conductor core, A.

Then according to current distribution:

$$I_s = I_t \left(\frac{R_c}{R_s + R_c} \right) \quad (4.6)$$

$$I_c = I_t \left(\frac{R_s}{R_s + R_c} \right) \quad (4.7)$$

From equations (4.6) and (4.7), the current distribution in one material of the composite conductor is a function of the temperature of both materials.

When conservation of energy equation (4.4) applied to both materials (core and conducting strands) the above equations become independent of each other.

$$\frac{k_s}{r} \frac{d}{dr} \left(r \frac{dT_s}{dr} \right) + \frac{I_s^2}{A_s} \frac{\rho_s}{A_{ms}} [1 + \alpha_s (T_s - 293)] = 0 \quad (4.8)$$

$$\frac{k_c}{r} \frac{d}{dr} \left(r \frac{dT_c}{dr} \right) + \frac{I_c^2}{A_c} \frac{\rho_c}{A_{mc}} [1 + \alpha_c (T_c - 293)] = 0 \quad (4.9)$$

where:

ρ = electrical resistivity at 20 °C

α = temperature coefficient of resistance

A = cross sectional area including air gaps, m^2

A_m = cross sectional area excluding air gaps, m^2

For composite conductor following boundary conditions applied:

1. $T(r) = T$ at $r = r_{os}$ Temperature at the surface is imposed

2. $T(r) = \text{Finite at } r = 0$ Finite temperature at the center of conductor
3. $T_s(r_{os}) = T_c(r_{os})$ Heat transfer at the interface of core & Al
4. Heat loss due to radiation and convection at the surface of the conductor must be equal to heat conducted through conductor.

The solution to equations (4.8) and (4.9) with boundary conditions mentioned above would be as follows:

$$T_{sc} = T_a [C_1 J_0((\frac{I_{sc}^2 \rho_{sc} \alpha_{sc} r_{sc}^2}{k_{sc} A_{sc} A_{msc}})^{1/2}) + C_2 Y_0((\frac{I_{sc}^2 \rho_{sc} \alpha_{sc} r_{sc}^2}{k_{sc} A_{sc} A_{msc}})^{1/2}) - (\frac{I - 293 \rho_{sc}}{T_a \alpha_{sc}})] \quad (4.10)$$

$$T_c = T_a [C_3 * J_0((\frac{I_c^2 \rho_c \alpha_c r_c^2}{k_s A_s A_{mc}})^{1/2}) + C_4 * Y_0((\frac{I_c^2 \rho_c \alpha_c r_c^2}{k_s A_s A_{mc}})^{1/2}) - (\frac{I - 293 \rho_c}{T_a \alpha_c})] \quad (4.11)$$

By forming series thermal circuit between the two layers of composite core material, the equation for temperature at the glass fiber material can be calculated as follows:

The glass fiber resistance is connected in series with the resistances of carbon core layer because the heat must flow consecutively through each material.

$$T_{sg} = T_{sc} + q_{cc} * \frac{(R_{sc} + \ln(r_{sg} / r_{os}))}{2 * \pi * k_g} \quad (4.12)$$

where:

T_{sc} = Temperature of the carbon material layer in the core, °C

T_c = Temperature of the conducting material (conductor surface temperature), °C

T_{sg} = Temperature of the composite core (carbon + fiber glass), °C

R_{sc} = Thermal resistance of carbon core material, Ω

r_{sg} = Radius of composite core material (carbon + glass fiber), Ω

r_{os} = Radius of composite core carbon material only, Ω

k_g = Thermal conductivity of fiber glass material

q_{cc} = Heat transfer rate in the glass fiber material

$C1, C2, C3$ & $C4$ = Constants of integration

J_0 & Y_0 = the zero order Bessel functions of the first and second kind.

The above equations were solved using the MATLAB program and results are presented in following section.

4.3 Computer Model

The computer code developed for the temperature distribution within the conductor requires the input of: the geometric, thermal and electrical properties for both the conducting and supporting materials and parameters which specify the thermal state of the environment. The geometric and thermal properties of the conductor which are needed include the outer radius of the supporting core, the diameter of supporting and conducting strands, the outer radius of the conductor, the absorptivity and emissivity of the conductor surface, and the effective thermal conductivities of the supporting core and the conducting layer. The electrical properties of the materials include the total current, the electrical resistivities and the temperature coefficient of resistance. Required environmental properties include the ambient temperature, the incident solar radiation, and the speed and direction of the ambient air. Another input value is an initial temperature estimate of both the conducting strands and the steel core. These temperature estimates are used to determine

values for R_g and R and then Equations 4.6 and 4.7 are used to calculate the current distribution in the conductor. Using the assumption that the current distribution is not significantly influenced by the temperature difference between the cores and supporting strands, the energy equations for both materials can then be solved independently. The computer model calculates a temperature distribution in the conductor based on this assumed current distribution. The model produces the temperature as a function of radius.

4.4 Analysis of Drake ACSR, ACCR and ACCC conductors

The computer model developed has been applied to Drake type ACSR, ACCR and ACCC conductors. The impact of the various parameters on the radial temperature distribution within the conductor was studied. A single input parameter was changed while keeping the other parameters constant. The typical physical characteristics of such conductors are listed in Table 4.1. The MATLAB program was used to calculate the radial temperature distribution for each of these conductors. The results for various conditions are presented in this section.

Table 4.1: Typical overhead conductor characteristics

Specification	ACCC Drake 1020 kcmil/517 mm²	ACCR Drake 795 (ACCR_824- T16)	ACSR Drake 795 (ACCR_824- T16)
Aluminum Cross section, kcmil	1020	795	795
Outside Diameter, mm	28.15	28.6	28.1178
Diameter of composite in core, mm	9.53	10.6	10.3632
Diameter of Al layer, mm	18.84	18	17.7546
Total cross section area of conductor, mm ²	588.1	484	468.644224
Actual Aluminum area, mm ²	517	418	403.031452
Total area, in ²	0.9116		0.7264
Total area, mm ²	588.1	484	468.644224
Conductor Al area, mm ²	516.9		403.031452
Composite core area, mm ²	71.225664		65.612772
Rated Total strength, lbs	41100	32200	31500
Aluminum strength, lbs	6540		NA
Composite core strength, lbs	34570		NA
Thermal expansion (CTE) of Al, /°C	2.30E-05	6.30E-06	NA
Thermal expansion (CTE) of core, /°C	1.61E-06	2.30E-05	NA
Thermal expansion of complete cable, /°C		1.65E-05	NA
AC Resistance at 25 °C	0.06	0.0674	0.0719
AC Resistance at 50 °C	0.50	0.0741	0.0796
Emissivity	0.50	0.5	0.5
Crosswind velocity, ft/s	2.00	2.933	2
Solar Absorption	0.50	0.5	0.5
Total solar & sky radiated heat, W/sq.ft	96.00		

Effect of Conductor Current: The Figure 4.2 shows the outer conducting surface temperature and the core temperature as a function of conductor current for ACSR, ACCR and ACCC conductors. The plot clearly shows that the temperature curve for ACCC conductors lies below ACSR and ACCR conductor curve.

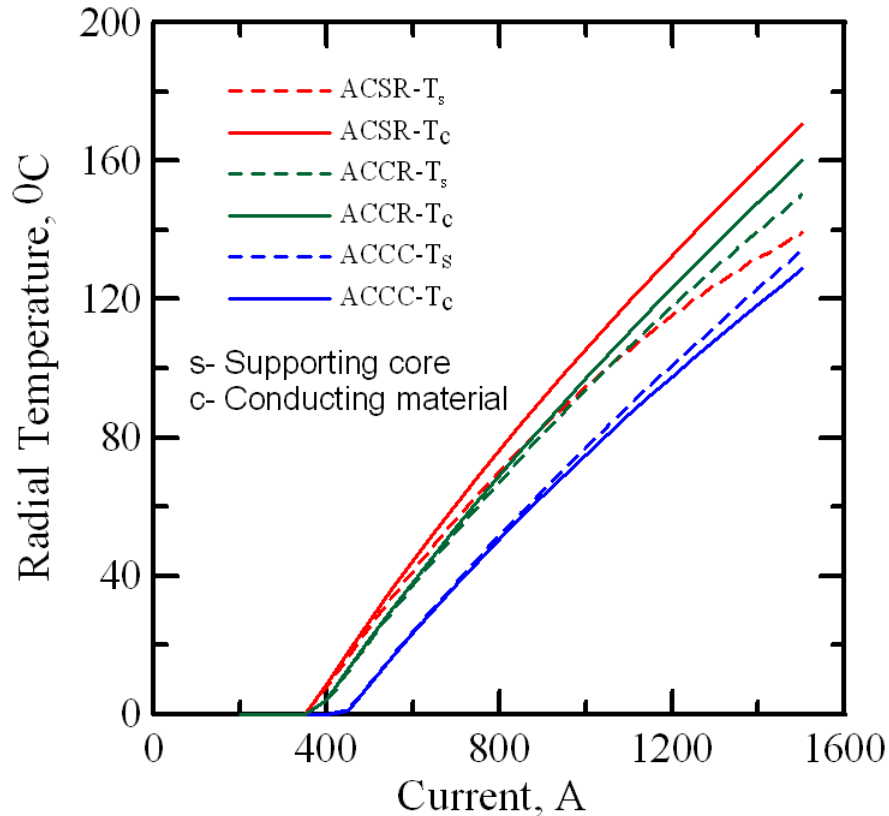


Figure 4.2: Surface temperature T_c and core temperature T_s as a function of current

Douglass [8] has compared the results of isothermal and non-isothermal model for several ACSR conductors. The temperature determined by the isothermal model for several ACSR conductors is within one percent of the outer surface temperature projected by the non-isothermal model. This fact, combined with the small size of the temperature gradients that exist within the conductor, help show that under normal operating conditions the conductor may be assumed isothermal with little or no impact on the accuracy of ampacity calculations [8].

Radial Temperature Difference as a Function of Conductor Current: Figure 4.3 shows the plot of radial temperature as a function of conductor current for Drake type ACSR, ACCR and ACCC conductors. The curves of ACCC & ACCR conductors lie under the ACSR conductor. The radial temperature difference is more for the case of ACSR conductors mainly due to resistance of the conductor and the air gap present in the adjacent strands. The radial temperature difference is more for the case of ACCC compared to ACCR mainly due to the fiber glass insulating material present in the composite core. The radial temperature difference at 1000 A current is less than 5°C.

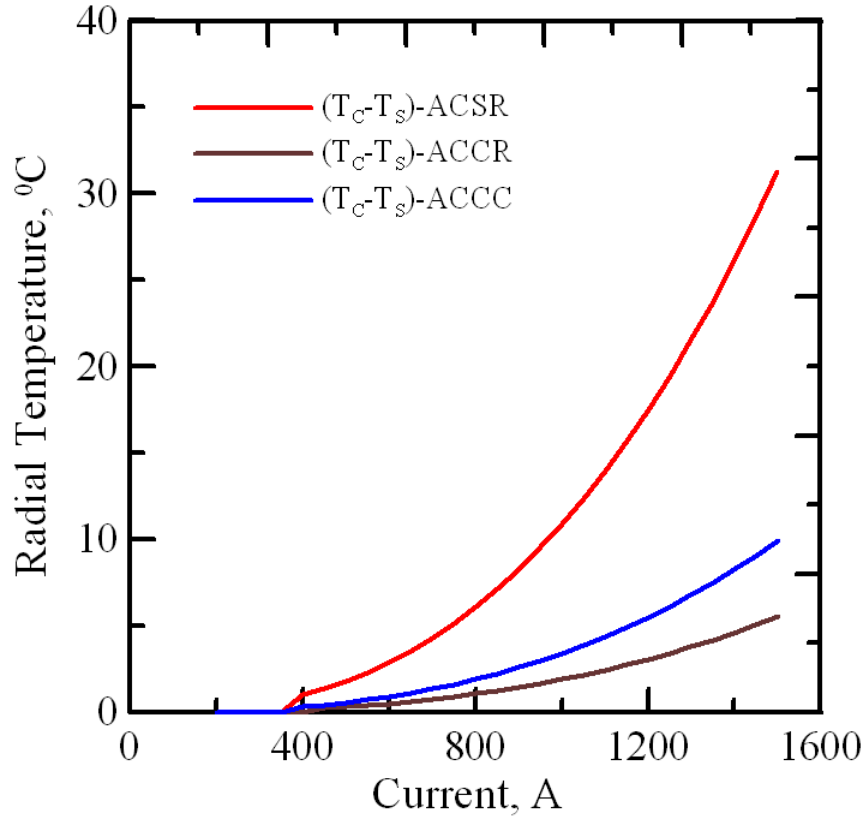


Figure 4.3: Radial temperature difference as a function conductor current

The radial temperature difference can become significant at higher conductor current as the heat generated within the conductor increases. Hence, conductor current is an important factor governing the radial temperature in the conductor.

Effect of Emissivity: The emissivity of a material is the ratio of energy radiated by a particular material to the energy radiated by a black body at the same temperature. It is a measure of a material's ability to radiate absorbed energy. Emissivity is dimensionless quantity. A true black body would have an emissivity value of $\varepsilon = 1$ while any real object would have $\varepsilon < 1$. The more reflective a material is, the lower its emissivity. Emissivity depends on factors such as temperature and emission angle.

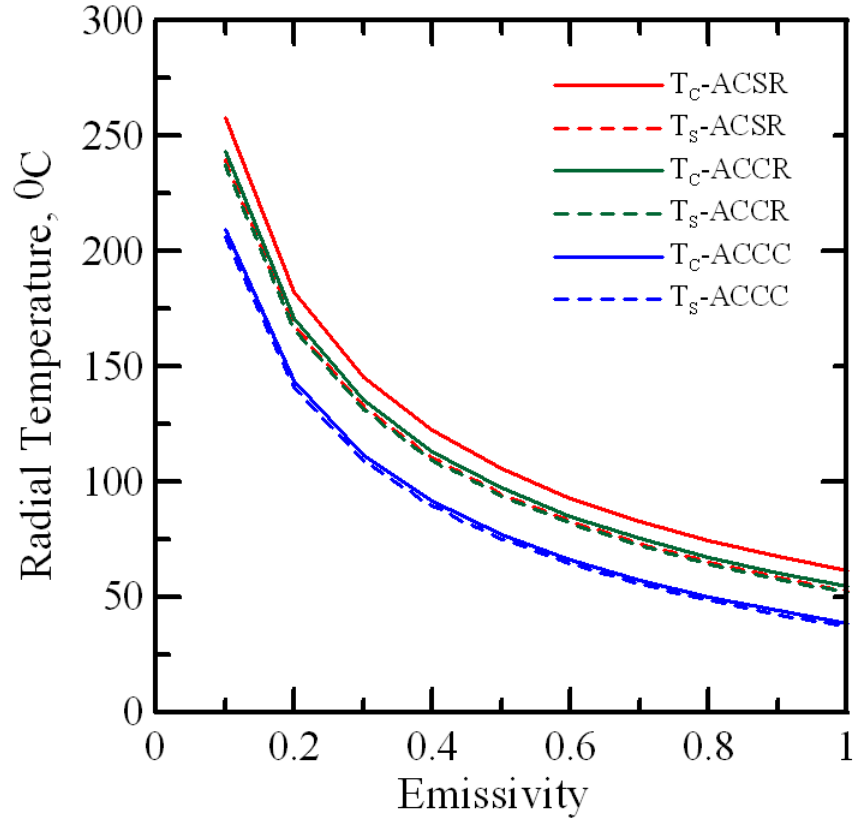


Figure 4.4: Temperature as a function of the emissivity (E) at conductor current $I=1000A$

The emissivity is treated as input and carried from 0.1 to 1. Figure 4.4 indicates decrease in radial temperature distribution as emissivity is increased. At low temperatures, radiation does not play as important a role as convection. This drop in radial temperature can be attributed to increase in the convective heat transfer coefficient. Above figure indicates that the radial temperature difference is insignificant and thus the emissivity of the conductor surface does not significantly affect the radial temperature difference within the conductor.

Effect of Thermal Conductivity: Thermal conductivity (k) is the property of a material that indicates its ability to conduct heat. Typical units are SI: $W/(m \cdot K)$ and English units: $Btu/(hr \cdot ft \cdot ^\circ F)$. Thermal conductivity depends on many properties of a material, notably its structure and temperature.

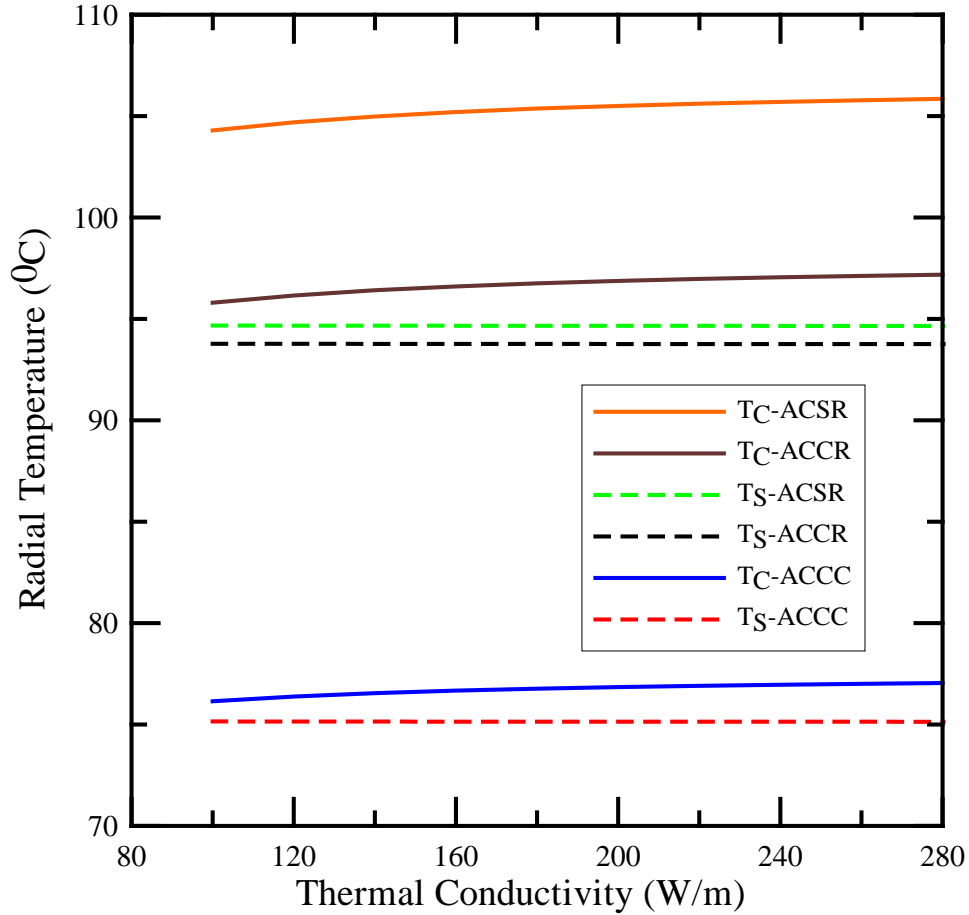


Figure 4.5: Temperature as a function of thermal conductivity of the outer conducting material at $I=1000A$

Air and other gases are generally good insulators, in the absence of convection. Therefore, many insulating materials function by having a large number of gas-filled pockets which prevent large scale convection. Figure 4.5 shows the radial temperature distribution within the conductor for various values of thermal conductivity. The plot indicates that varying the thermal conductivity of the outer conducting material does not significantly affect the outer surface temperature. However it does have a slight effect on the radial temperature difference. This difference ($18^{\circ}C - 20^{\circ}C$) is significant for ACSR conductors compared to ACCR ($4^{\circ}C - 8^{\circ}C$) and ACCC ($2^{\circ}C - 6^{\circ}C$) conductors.

Effect of Ambient Temperature: Figure 4.6 shows the relationship between conductor temperature and ambient temperature. In actual operating conditions the ambient temperature could range between $0^{\circ}C$ to $40^{\circ}C$.

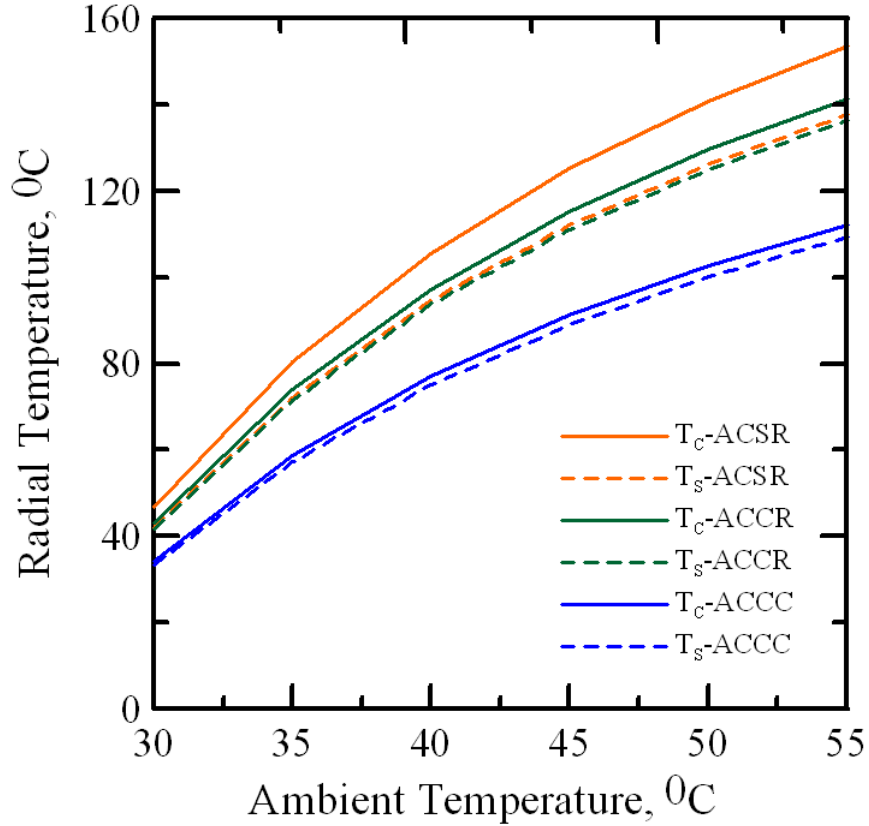


Figure 4.6: Temperature as a function of an ambient temperature (T_a) for $I=1000A$

Figure 4.6 shows that there is a slight increase in radial temperature difference as ambient temperature increases. This increase in radial temperature difference is due to an increase in resistance at high temperatures.

Other than resistivity, the only two conductor variables affecting conductor temperatures are emissivity and absorption. Emissivity is defined as the ability of a conductor to radiate heat to its surroundings. Absorptivity is the ability of a conductor to absorb heat from its surroundings. Both emissivity and absorptivity are dependent upon conductor surface conditions and increase from about 0.2 to 0.9 with conductor age [15]. The exact rate of increase depends on the level of atmospheric pollution and the line's operating voltage. Generally, the absorptivity is higher than the emissivity over the life of the conductor, although both values increase with age and atmospheric pollution.

5. Study of IEEE Standard – 738 for Calculating the Current-Temperature of Bare Overhead Conductors

5.1 Introduction

This chapter discusses the various components of static tensile testing system, uniaxial tensile response of carbon composite core and metal matrix core used in overhead conductors at two temperatures. The components of the test setup in addition to test procedure, data reduction approaches and material property calculations are described. The testing system includes INSTRON 55 *kips* hydraulic test frame operated under closed-loop conditions, force measurement and data acquisition system. The carbon composite and metal matrix cores were tested at room temperature and elevated temperature.

The tensile strength of Drake size carbon composite core was measured at room temperature and 210°C. This test was conducted to see the effect of temperature on tensile load of core. The temperature of 210°C was selected as an overhead conductor is designed for a continuous temperature of 210°C. An emergency use rating for composite overhead conductor is 240°C [2]. The results of tests conducted at room temperature and 210°C are compared for analysis. The sample was subjected to a temperature of 210°C for one hour prior to the test to failure. Also few samples were subjected to a temperature of 210°C and 240°C for 120 hrs before conducting tensile test to determine the short term and long term effect of temperature. The average tensile strength at 27°C was 29000 *lbf* (128.998 *kN*). At 210°C the average strength was 74% of the tensile strength of the composite core at room temperature. However this strength is well above the required strength in field. The operating range of these conductors is expected to be between 100°C to 210°C with short term maximum operating temperatures tolerated to 240°C. There is a concern about potential loss of strength due to matrix degradation and attempt has been made to address this issue in this chapter.

5.2 Test Setup and Procedure

Tests were conducted in a 55 *kips* servo-hydraulic test frame operated under closed-loop control. The testing system, as shown in Figure 5.1, includes INSTRON 5 *kips* servo-hydraulic tensile testing machine, data acquisition system.



Figure 5.1: Tensile testing system

Schematic Diagram of this testing system is as shown in Figure 5.2.

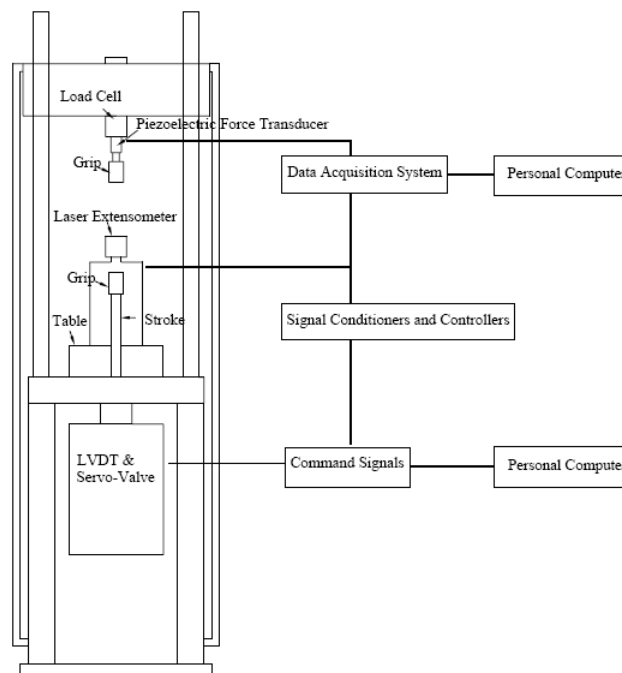


Figure 5.2: Schematic diagram of test system

Tensile Test Grips: A new gripping system for static tests was designed using internal wedges that were held inside the female portion of screw connectors. The grip wedges and gripping arrangement are shown in Figure 5.4 and Figure 5.4-5.5. The total weight of the grip system is 7.57 lb. Four steel wedges (1.0" wide, 2" long) are used to grip the specimen at both ends.

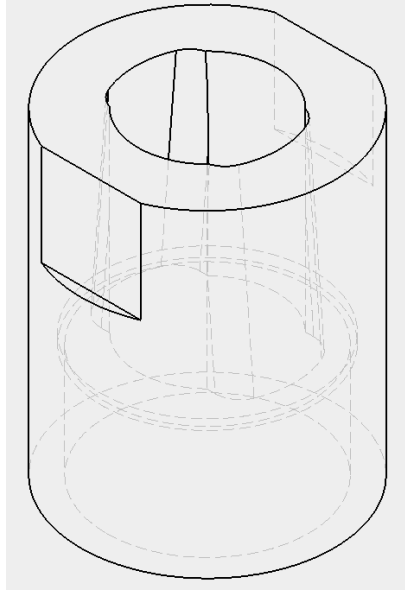


Figure 5.3: 3-D view of a main body of cylindrical grip

The entire length of the wedge grip faces was serrated in order to improve the contact with the test specimen. These wedges are housed inside hollow connecting rods. The grip was tightened by turning the screw assembly that pushes the grip against two slanted surfaces inside the wedge. Furthermore, care must be exercised to ensure that there is no relative sliding of the two faces of the grip as the wedge components slide and tighten. In order to ensure that slipping of the specimens (from the grips) did not influence the deflection values, the gripping fixture (Figure 5.5) developed was used as shown in Figures (5.4-5.6).

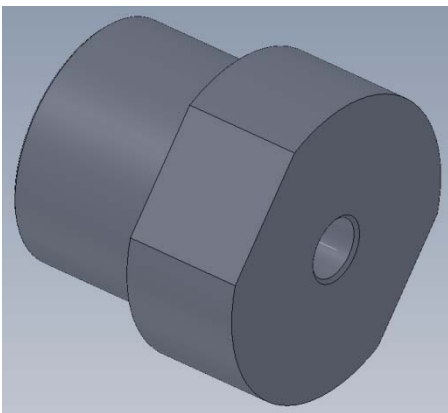


Figure 5.4: end cap of cylindrical grip

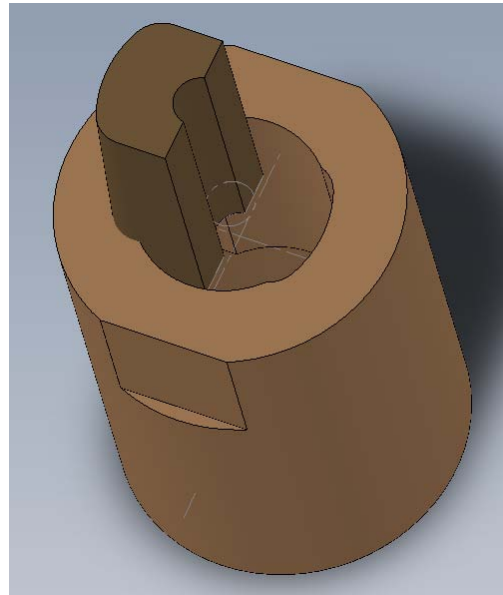


Figure 5.5: Cylindrical grip with tapered wedge

Experimental Setup and Procedure: The ultimate tensile strength of Drake size composite core as a function of temperature was determined at room temperature and elevated temperature of 210°C. Samples were mounted in custom grips as shown in Figure 5.6. The samples were heated for 1hr prior to loading to failure at 210°C. Then end caps of the wedge tool were placed in the hydraulic grips of the INSTRON tensile testing machine.

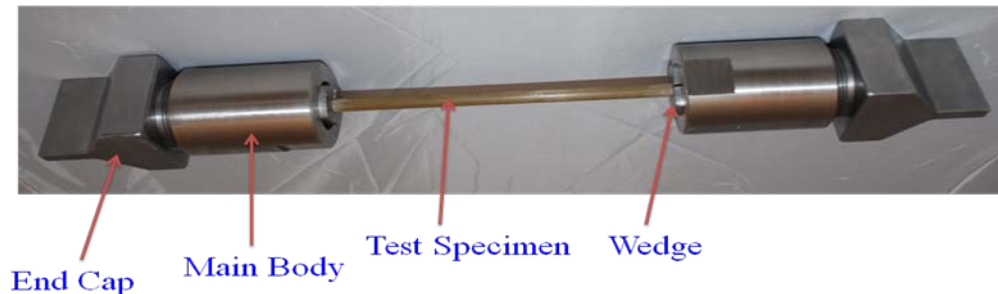


Figure 5.6: Carbon composite core with cylindrical grips

The test procedure was a displacement control test with the rate of displacement of actuator (stroke) set at 0.1"/min and sampling frequency of 2 Hz. Digital data acquisition was used to collect data at every 0.5 second. The test was continued until complete failure of the specimen was achieved. The load-deformation results were used to calculate the stress-strain response. However, there were couples of challenges faced during tensile testing of carbon composite rods as shown in Figure 5.7.

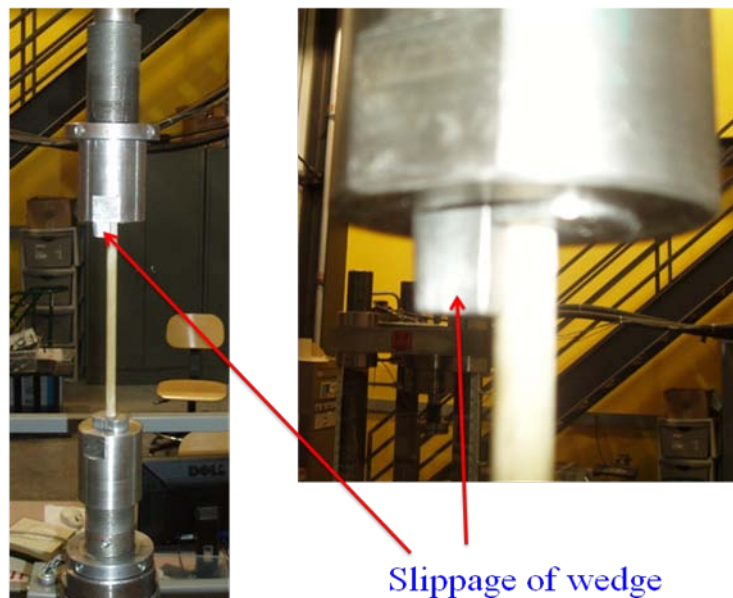


Figure 5.7: Carbon composite core tensile test setup

The slippage of one of the wedge was major obstacle with cylindrical grips and subsequently slipping carbon composite rod from the wedges. To overcome this problem improved design of grips is shown below in Figure 5.8.

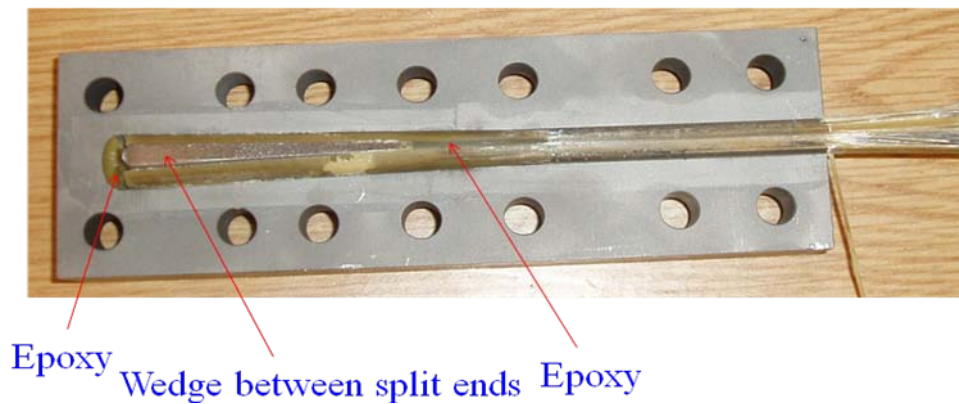


Figure 5.8: Carbon composite core with rectangular grip with wedge in split end grip tool

These grips are referred as rectangular grips in this report. The grips are made out of tool steel in which a hole has been cut out of them with a certain taper to form a cone inside the grip. The grip consists of two pieces, each with a machined cone that mirrors the other side. The two sides are bolted together with screws to form the grip. Two smaller holes have been drilled into one side of the grip, for which the epoxy is injected into the grips when they are sealed.

To test the tensile strength of the carbon composite rod, the ends of the rods are split into two section and placed into aluminum grips. The metallic wedge was placed in between split ends which prevents the axial movement of core inside the grips. Epoxy is injected into these grips which sets the composite and transfers the tensile loads from the grips into the gauge section of the composite.

The following details the procedures for fixing the composite rods into these aluminum grips

1. The carbon composite rod is cut in to 24 inches in length. The ends of the rod (4 inch) are split into 2 prongs on diamond cutter machine.
2. The carbon composite rods are then set into the grips. The metallic wedge is placed between the split ends.
3. With the grips still open, the screws are put into the bolt holes of one side of the grip. The prepared carbon composite rod is then laid into the open grips, with the split end of the rod made to touch the end of the cone.
4. The other half of the grip is then laid down on top of the lower grip and is aligned by the screws coming up for the lower grip.
5. A washer and nut is then screwed onto the end of the exposed screws. All the screws are then tightened as much as possible to seal the grips.
6. With the grips sealed, the grips are laid on the bench to expose the epoxy injection holes. The epoxy resin and hardener are poured into separate bowl in a 1:1 ratio, respectively. The stirrer is used to mix resin and hardener properly.
7. Syringes are then filled with mixture of epoxy and hardener. The epoxy is then injected into the grips at the hole drilled into the top of the cone. The epoxy is slowly injected into the grip until the epoxy comes out of the hole located at the end of the taper. Any epoxy that comes out of these holes is then wiped away

8. The procedure is then repeated for the grip on the other end of specimen. The epoxy is then allowed to cure at room temperature for at least 24 hours before testing.
9. The specimens are loaded into an INSTRON test machine as shown in Figure 5.7. The rod is marked with a permanent marker at the carbon composite rod and grip interface so that it can be observed how far the carbon composite rod is being pulled out of the grip during the test.

Tensile Test at Room Temperature: A computer is attached to the load frame which controls the operation of the frame. The MTS testing software is programmed to run the test frame at the desired loading rates. The software records the position of the lower crosshead, the extensometer measurements and the load. The sample is then loaded at 0.10 inches/min until failure. After the sample has failed, the sample is removed from the test frame and pictures of the results are taken. The test data file from the MTS testing software is then read into Excel and graphs are plotted using Grapher 4 software. The test data file includes the time, the strain, stress, load and crosshead position.

Tensile Test at Elevated Temperature: Tensile test at elevated temperatures is done under the same conditions as described in above section except that heating tape is wrapped around the composite rod. The heating tape is supplied with 120V AC supply and then adjusted to the desired temperature. The composite rod is heated at the desired temperature for 1 hour prior to testing to failure of the sample. Test setup is as shown in Figure 5.9.

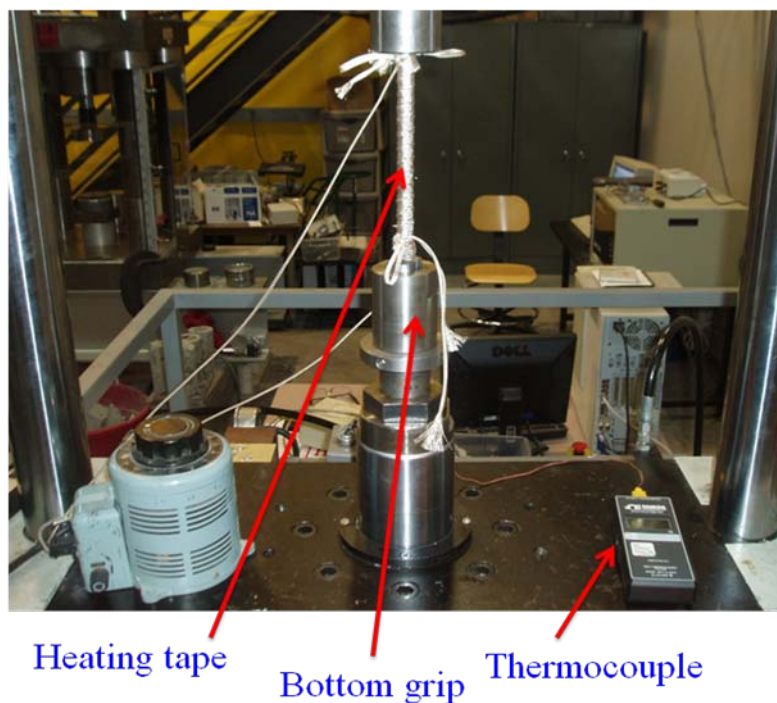


Figure 5.9: Tensile test setup at elevated temperature.

5.3 Test Results

Test data from the tensile tests are affected by various sources of noise in the experimental set up. The test data may include transducer noise and mechanical vibrations that should be separated from the test data. Linear interpolation method was used to smooth the deformation data measured by LVDT/stroke. The stroke velocity was the slope of the smoothed deformation versus time curve. Based on the linear deformation versus time curve, stress versus strain curves were computed over the test duration. Both strain rate and stress versus strain curve were computed based on LVDT/stroke measurement. The tensile test result data is shown below for two temperatures in Table 5.1.

Table 5.1: Tensile test results

Parameter	Test at room temperature	Test at 210°C temperature
Average maximum load, <i>lbf</i>	29550	21750
Modulus, <i>E</i> , <i>MPa (psi)</i>	48667.68 (7058650)	39213.656 (5687460)
The toughness, <i>lbf-in</i>	12116	7175
Average strength, <i>MPa (psi)</i>	1844.64 (267542)	1357.73 (196922)
Average maximum stress, <i>in/in</i>	0.0765	0.0626

Note:

- (a) Stress is obtained by dividing the peak load by the cross-section area of specimen.
- (b) Maximum strain is obtained by dividing maximum displacement by the gauge length of specimen.
- (c) Toughness is calculated by the area under the stress-strain curve.

The failure of all carbon composite rods was observed in the gauge section and is shown in Figure 5.10 below.

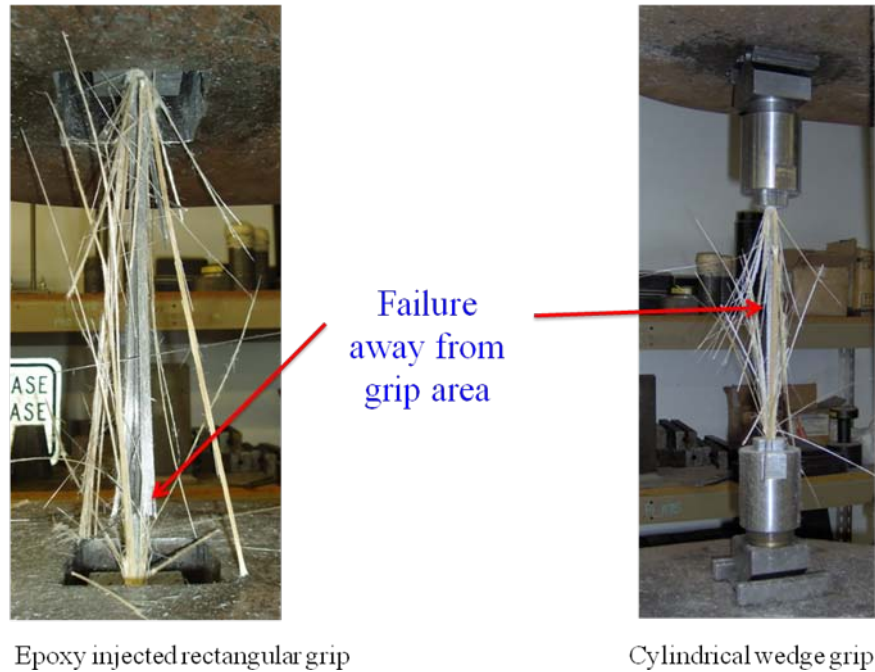


Figure 5.10: Tensile test failed samples with different grips

5.4 Analysis of Test Results

Test data was analyzed to:

- Understand the fundamental tensile response of carbon composite core under uniaxial loading
- Provide estimation of tensile stiffness and strength
- Document the effect of temperature on failure stress.
- Compare the tensile properties at room and elevated temperatures
- Ageing model using Weibull distribution

The slippage data was captured and Figure 5.11 shows the slippage of wedge around 8000 *lbf* load value. To overcome these problem rectangular grips with epoxy injection were designed as discussed above.

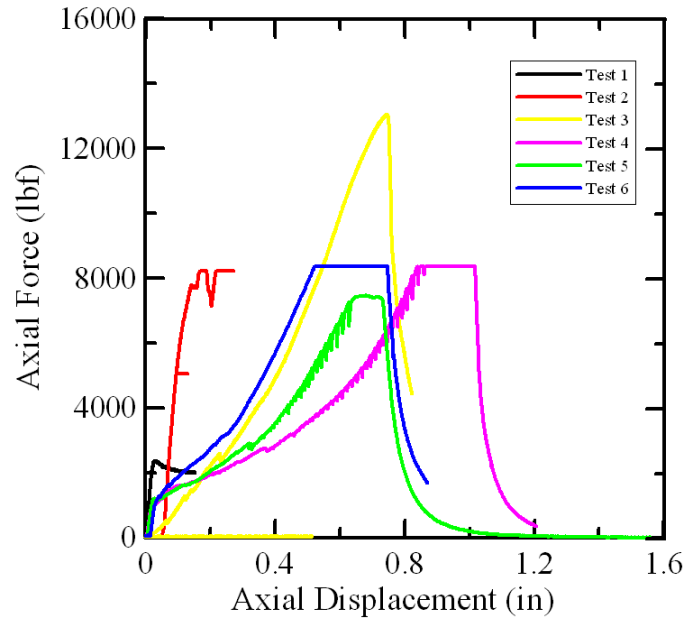


Figure 5.11: Test failure due to one of the wedge slipping from cylindrical grip

Stress-Strain Curve for test conducted at room temperature is shown in Figure 5.12.

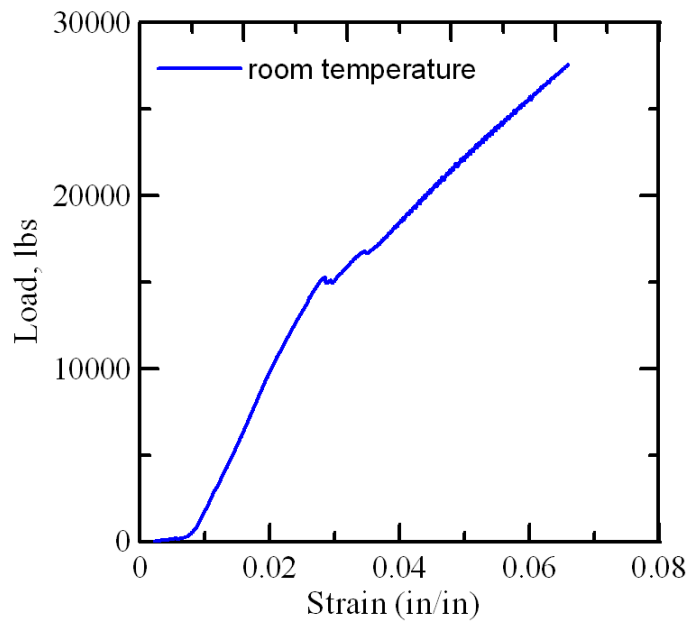


Figure 5.12: Stress-Strain curve at room temperature

Maximum load, $lbf = 29550$; Modulus, $E, psi = 7058650$
 The toughness, $lbf \cdot in = 12116$; Strength, $psi = 267542$

Stress-Strain Curve for test conducted at elevated temperature is shown in Figure 5.13.

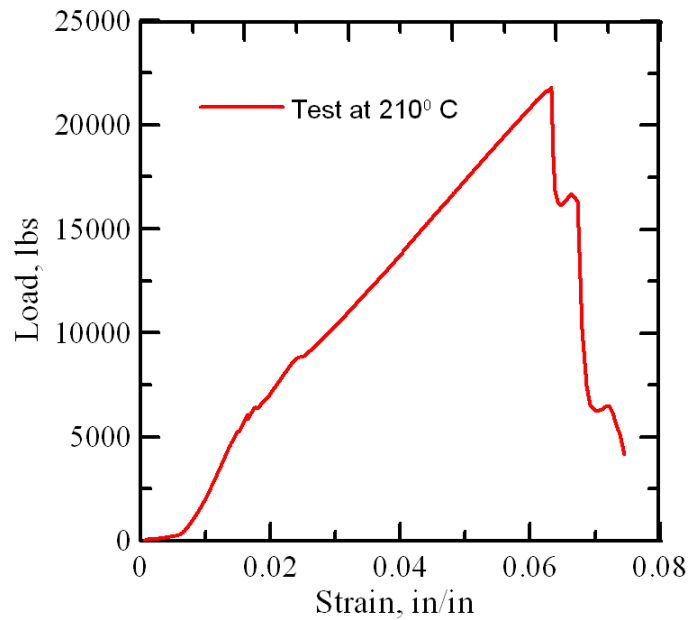


Figure 5.13: Stress-Strain curve at elevated temperature

Maximum load, f , $lbf = 21750$; Modulus, E , $psi = 5687460$
 Toughness, $lbf \cdot in = 7175$; Maximum stress, $in/in = 0.0626$

The comparison of stress-strain curve for two temperatures is shown in Figure 5.14. It was observed that tensile load reduced by 26.40% when sample was heated at 210°C for 1hr before the test up to failure.

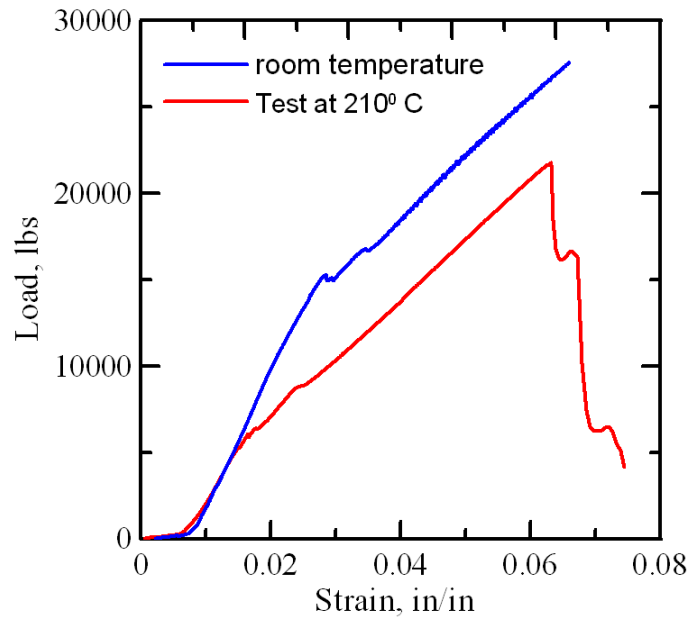


Figure 5.14: Comparison of Stress-Strain curve for two temperatures

5.5 Weibull Statistics

Two most important characteristics of any reinforcement material are its strength and Young's modulus. All these high performance reinforcements (fibers, whiskers, or particles) have very low density values. Fiber flexibility is associated with the Young's modulus and the diameter. Some fibers have quite anisotropic characteristics. The strength, modulus, and thermal characteristics can vary with direction, especially along the fiber axis and transverse to it. In particular, the thermal expansion coefficient of carbon is quite different in the radial and longitudinal directions. The polycrystalline fibers such as Al_2O_3 fibers are reasonably isotropic. Another important characteristic of these high performance fibers is their rather low values of strain-to-fracture, generally $< 2-3\%$ [16].

The classical way to view the strength of the materials or structures is a deterministic one. That is, a true strength, a single value that is characteristic of the material or structure, is supposed to exist. In experiments to determine this true strength, considerable scatter in the results is usually observed. As this is not considered to be a feature of the material or object itself, it is usually attributed to uncontrollable experimental variables. As a consequence, the second central moment of the experimental data, the standard deviation, is interpreted as indicating the success of standardizing the experimental set-up and procedures. Therefore, standard deviation can be considered to be an indicator of the quality of an experiment or testing method. The deterministic view has become much less popular in the technical sciences. If the deterministic view is valid, identical experiments performed on material specimens of different sizes should yield the same results for failure stress.

We can regard a fiber of a given length to be made up of a series of chain links. When such a fiber is loaded, the link or the segment containing the longest defect will fail first and cause the fiber to fracture. The longer the fiber, the higher the probability of a link having a critical flaw size required for failure. In other words, one would expect that the mean strength of a short fiber length to be greater than the mean strength of a long fiber length. The fiber failure occurs when the weakest link fails. This is called the weakest-link assumption. It turns out that such a "weak-chain" material is well described by a statistical distribution known as the Weibull distribution, named after the person who first proposed it (Weibull, 1959). The basic assumption is that a fiber has a distribution of flaws (on the surface and/or in the interior). The Weibull distribution assumes that all segments or chain links have the same type of flaw but of different lengths. Such a "weak-link" material is well described by a statistical distribution known as the Weibull distribution. The Weibull distribution is a parametric distribution, i.e., it is an empirical distribution and does not concern itself with the origin of the defects.

However, it has been shown that fiber strength is a statistical quantity since it is governed by the propagation of pre-existing flaws or cracks in the fiber [16]. Typically, statistical fiber strength distributions are measured directly by performing single-fiber tension tests on a collection of fibers at a common gage length L . In such a test, the fiber stress is uniform across the fiber cross-section and uniform along the length of the fiber within the gage section. The strength data obtained from such a test are usually characterized in terms of a Weibull probability distribution, wherein the cumulative probability of failure of a fiber of length L at stress σ is given by:

$$P_f(\sigma, L) = 1 - \exp \left[-\frac{L}{L_0} \times \left(\frac{\sigma}{\sigma_0} \right)^m \right] \quad (5.1)$$

Where σ_0 is the characteristic fiber strength at gauge length L_0 and m is the Weibull modulus characterizing the spread in the distribution of strengths at any gage length.

To calculate the Weibull modulus, two additional values must be computed, the natural logarithm of the stress and the natural logarithm of the natural logarithm of the following equation:

$$\frac{N+1}{N+1+i} \quad (5.2)$$

Where N is the total number of tests and i is the current test specimen. Therefore, there will be a corresponding relation for each test. The slope of the plot of the $\text{LN}(\text{stress})$ against the $\text{LN}(\text{LN}(N+1/N+1+i))$ will give us the Weibull modulus of the tests.

Experimentally, to obtain the Weibull parameters, one tests a series of identical samples (each of same volume, or in the case of fiber of constant diameter, each of a constant length) to failure. From such tests we can obtain the fraction of samples that survives, $P(\sigma)$, when loaded to a given stress, σ .

Unidirectional Analysis Specific Considerations: Juan Erni [17] has developed a computational analytical model based on the strength failure criterion mixed with the Weibull Statistics. It uses the Weibull failure probability function (equation (5.1)) to calculate the corresponding distribution of failure stresses, and a random distribution function to assign those stresses among the plies that compose the laminate. As an example of the model behavior, a stress-strain plot is shown in Figure 13 and the corresponding Weibull function is plotted in Figure 5.17. The simulation procedure is as follows:

1. Definition of the geometry (number of layers, cells, thickness, orientation of the lamina (if necessary), etc) for the composite laminate.
2. Definition of the composite material elastic properties (E_1 , E_2 , ν_{12} , ν_{21} , G_{12}), where these properties are a function of the fiber and matrix properties.
3. Definition of the strength values for the specific failure criteria (S_{1T} , S_{2T} , S_{12} , etc.).
4. Calculation of the orthotropic stiffness matrix components according to the following equations:

$$\begin{aligned} Q_{11} &= \frac{E_1}{1 - \nu_{12} \times \nu_{21}} & Q_{22} &= \frac{E_2}{1 - \nu_{12} \times \nu_{21}} \\ Q_{12} &= \frac{\nu_{12} \times E_2}{1 - \nu_{12} \times \nu_{21}} & Q_{66} &= G_{12} \end{aligned} \quad (5.3)$$

5. Assignment of the randomly statistical strength, or other related value, to each layer or cell; this step depends on the failure criteria. This statistical approach is based on the Weibull model for probability of failure detailed in section 3.6.
6. Incremental strain is applied, and the constitutive behavior of each lamina will calculate its respective stress level in global (x-y) coordinates.
7. According to the corresponding failure criteria and/or statistical criteria, the strength or failure value will be check and if failure occurs the layer or cell stiffness will be significantly reduced for the next step.

8. Depending on the complexity of the model, a load sharing rule will be applied on the neighbor lamina or cells. Equilibrium on the section will be maintained.
9. Border effects are related to the load sharing rule and will be taken into account only in the y-direction.
10. If failure occurs in the lamina or cells affected by the load sharing rule, they will follow the same procedure shown on step 8.
11. Accumulation of the stress for each lamina or cell, then we will return to step 7, adding the incremental strain and evaluate the laminate with the updated stiffness.

A MATLAB code available at civil engineering department, ASU that employs the least squares approach to get the Weibull characteristic stress, found the value to be 1522 MPa ; and with that characteristic stress calculated and the Weibull modulus of 5.187 the plot of the Weibull failure distribution for carbon composite fibers is shown in Figure 5.15.

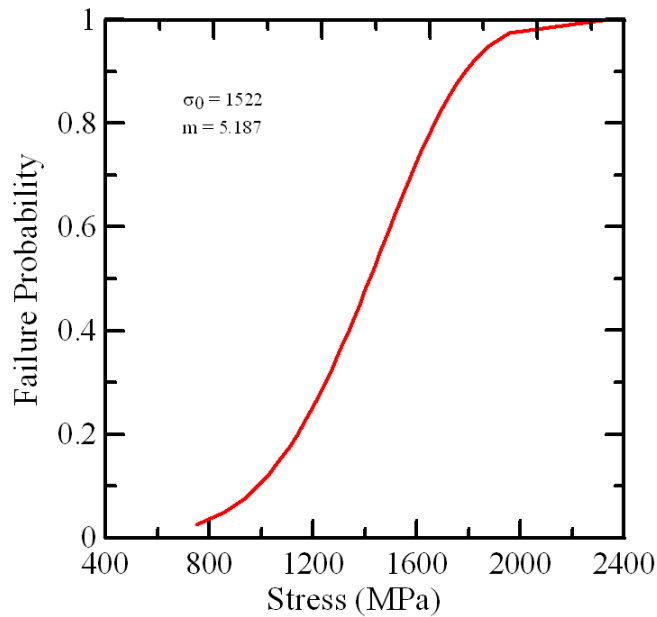


Figure 5.15: Failure probability curve for carbon composite core

Weibull stress-strain curve for tests conducted on carbon composite core samples in laboratory for Weibull modulus, $m = 5.187$ and $\sigma_0 = 1522 \text{ MPa}$ is shown in Figure 5.16.

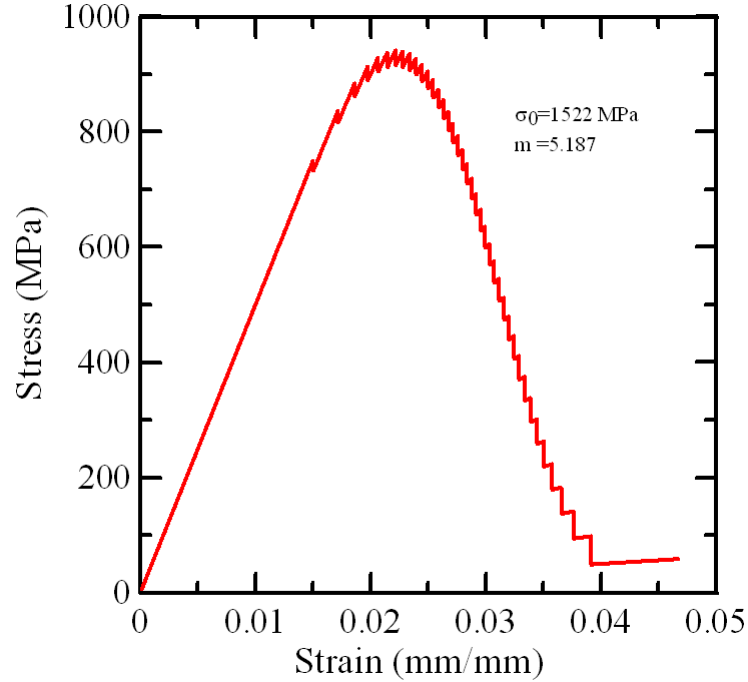


Figure 5.16: Weibull stress-strain curve for carbon composite core

The second model additionally uses a simplified load sharing rule applied on steps 8, 9 and 10 of the algorithm. This rule specifies that once a failure happens, two layers above and two layers below will suffer an increase of the load, which will increase the chance of failure and the possibility of an accumulated failure region in the laminate. Border conditions were taken into account, if the failure happens near and/or at the edges (y-direction) the neighbor plies will have an additional increment in the load. Figure 5.17 shows axial stress distribution for carbon composite fibers.

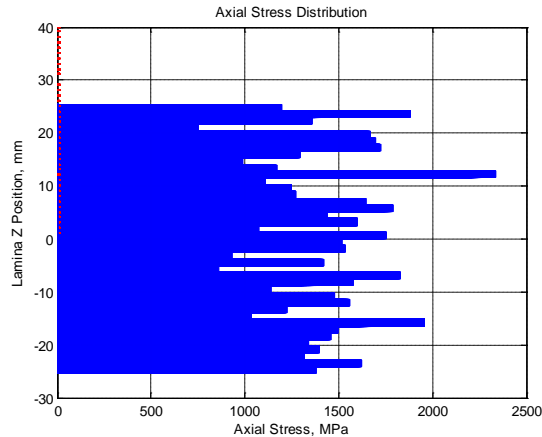


Figure 5.17: Axial stress distribution for carbon composite core,
Weibull values $\sigma_0=1522$ MPa, $m=5.187$

Failure Curve (Ageing Model): As Weibull modulus, m , increases, the distribution becomes less broad. In general, brittle materials have a lower Weibull modulus than ductile materials. The

Weibull modulus, m is a measure of the variability in the strength of the fiber. Higher the value of Weibull modulus, higher is the uniformity of strength values. The Weibull modulus, m , is a measure of the flaw distribution in the sample. The smaller the value of m , greater is the variability in strength.

Table 5.2: Typical Weibull modulus (m) values for materials in fibrous form (inspired from [16])

Fiber Material	Weibull Modulus, m (values only)
Glass	< 5
SiC, Al_2O_3 , C, B	$5 - 10$
Steel	>100

The failure probability curve as a function of fiber stress for different values of m is shown in Figure 5.18.

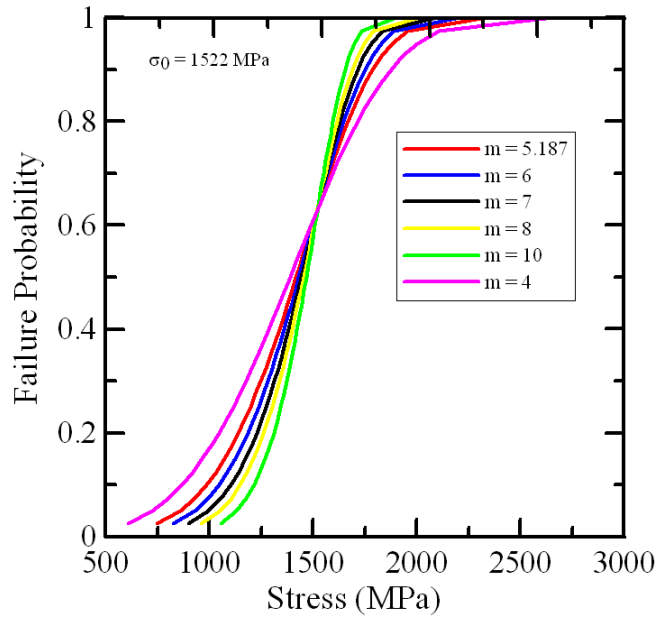


Figure 5.18: Failure probability curve for carbon composite core (for different values Weibull Modulus, m)

The stress-strain curve for different values of Weibull modulus, m , is also shown in Figure 5.19. Table 2 shows typical Weibull modulus for several fibers.

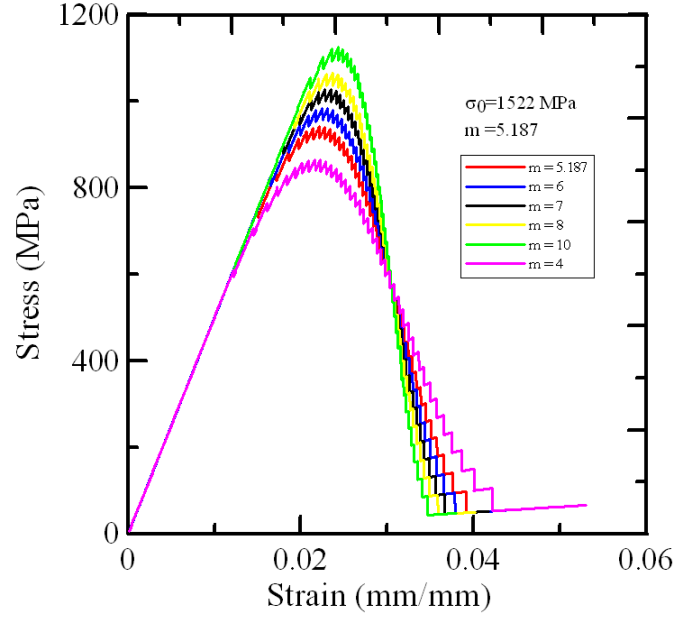


Figure 5.19: Weibull stress-strain curve for carbon composite core (for different values of Weibull Modulus, m)

As indicated in Figure 5.19 as the Weibull modulus, m decreases there is a reduction in tensile stress of composite core. The Weibull modulus decreases as composite cores are subjected to elevated temperatures.

The performance of carbon core under two temperatures was studied by conducting tension stress-strain test. The tension test fixture was developed for a carbon composite core. The experimental data was modeled using a back calculation procedure to measure effect of temperatures and ageing on the strength of fibers based on Weibull distribution.

6. Conclusions and Future Work

6.1 Conclusions

This work deals with an evaluation of composite cores in ACCR & ACCC conductors. In this approach, detailed radial temperature model for composite conductor and tensile test fixture for conducting tensile tests on carbon composite cores were developed.

The mathematical model for radial temperature gradient in ACCC conductor was developed and its results were found to be comparable to the results obtained from the manufactures specification sheet and other models [13] available in the field. The steady state solutions for the differential equation are given for the composite conductor ampacity and temperature calculation. The radial temperature differential in the composite conductor due to surface temperature and composite core temperature is derived. The maximum radial temperature difference, that exist in typical ASCR conductor for reasonable weather conditions and conductor temperature less than 150°C is not more than 8°C [13]. The radial temperature differences of 1–6 °C were observed for ACCC conductors. The radial temperature difference in ACCC conductors is less than that of ACSR conductors. MATLAB program for steady state temperature and radial temperature calculation of ACCC conductors are presented with various plots and compared with ACSR conductor plots.

Following results were observed for the various tests conducted in the laboratory:

- Metal matrix core does not show significant reduction in strength in tensile strength at elevated temperature.
- Some batches of carbon composite core show cracking.
- At elevated temperature carbon composite core show 26% reduction in tensile strength however this is greater than required value.
- Thermal model predicts that radial temperature difference in metal matrix conductor is less than that of carbon composite conductor.
- The tensile strength data obtained from laboratory test was characterized in terms of a Weibull probability distribution to understand core ageing.

6.2 Future Work

The analysis done in this thesis largely consisted of examining the performance of the composite cores at elevated temperature for Drake type conductors. .

The future works in a related area are:

- Role of long term elevated temperature on mechanical strength.
- In depth study of mechanisms leading to reduction in mechanical strength.
- Validation of theoretical model results.
- Correlation between formulation & processing on the cracking of carbon composite core.

References

- [1] A. Alawar, E. J. Bosze, S. R. Nutt, "A Composite Core Conductor for Low Sag at High Temperatures," IEEE Transactions on Power Delivery, July 2005, Vol. 20, No. 3, pp. 2193-2199.
- [2] Anonymous, "Aluminum Conductor Composite Reinforced Technical Notebook (477 kcmil family)," 3M, November 2006,
- [3] V. Filipovic-Gledja, V. T. Morgan, R. D. Findlay, "A Unified Model for Predicting the Electrical, Mechanical and Thermal Characteristics of Stranded Overhead-Line Conductors," Electrical and Computer Engineering, 1994 Conference Proceedings, 25-28 September 1994, Vol. 1, pp. 182-185.
- [4] W. Z. Black, W. R. Byrd, "Real-Time Ampacity Model for Overhead Lines," IEEE Transactions on Power Apparatus and Systems, July 1983, Vol. PAS-102, No. 7, pp. 2289-2293.
- [5] V. T. Morgan, "The Radial Temperature Distribution and Effective Radial Thermal Conductivity in Bare Solid and Stranded Conductors," IEEE Transactions on Power Delivery, July 1990, Vol. 5, No. 3, pp. 1443-1452.
- [6] V. T. Morgan, R. D. Findlay, "Effects of Axial Tension and Reduced Air Pressure on the Radial Thermal Conductivity of a Strained Conductor," IEEE Transactions on Power Delivery, April 1993, Vol. 8, No. 2, pp. 553-558.
- [7] W. Z. Black, R. L. Rehberg, "Simplified Model for Steady State and Real-Time Ampacity of Overhead Conductors," IEEE Transactions on Power Apparatus and Systems, October 1985, Vol. PAS-104, No. 10, pp. 2942-2953.
- [8] D. A. Douglass, "Radial and Axial Temperate Gradients in Bare Stranded Conductor," IEEE Transactions on Power Delivery, April 1986, Vol. 1, No. 2, pp.7-15.
- [9] IEEE, "IEEE Standard for Calculating the Current-Temperature of Bare Overhead Conductors," IEEE Std. 738-2006, January 2007.
- [10] R. S. Gorur, N. Chawla, J. Hunt, M. Dyer, "Mechanical and Electrical Issues Concerning the Use of Composite Materials for the Supporting Core in Transmission Line Conductors," Electrical Insulation and Dielectric Phenomena 2006, IEEE Conference on Power Delivery, 15-18 October 2006, Vol. 3, pp. 501-504.
- [11] A. E. Kennelly, F. A. Laws, P. H. Pierce, "Experimental Researches of Skin Effect in Conductors," AIEE Transactions, 1915, Vol. 34, Part 2, pp. 1953-2021.
- [12] Southwire, "Southwire Overhead Conductor Manual,"
- [13] W. Z. Black, S. S. Collins, J. F. Hall, "Theoretical Model for Temperature Gradients within Bare Overhead Conductors," IEEE Transactions on Power Delivery, April 1988, Vol. 3, No. 2, pp. 707-715.
- [14] F. Keith, W. Black, "Basic Heat Transfer," Harper & Row, Publishers, New York, 1980.
- [15] C. S. Taylor, H. E. House, "Emissivity and its Effects on the Current Carrying Capacity of Stranded Aluminum Conductors," AIEE Transactions, October 1956, Vol. 75, Part. II, pp. 970-976.
- [16] N. Chawla, K. K. Chawla, "Metal Matrix Composites," Springer, USA, 2006.

- [17] J. Erni, "The Development of Unidirectional and Multidirectional Composite Models Using a Modified Weibull Failure Distribution: Theory, Analysis and Applications," Arizona State University, December 2007.
- [18] P. Shrestha, K. Pham, "A Computer Program to Perform Dynamic Thermal Analysis for Bare Overhead Conductors during Short-Time Overload Conditions," IEEE Technical Applications Conference and Workshops Northcon95, 10-12 October 1995, Vol. 1, pp. 207-212.
- [19] G. A. Davidson, T. E. Donoho, P. R. Landrieu, R. T. McElhaney, J. H. Saeger, "Short-Time Thermal Ratings for Bare Overhead Conductors," IEEE Transactions on Power Apparatus and Systems, March 1969, Vol. PAS-88, No. 3, pp. 194-199.
- [20] O. R. Schurig, C. U. Frick, "Heating and Current Carrying Capacity of Bare Conductor for Outdoor Services," General Electric Review, March 1930, Vol. 33, No. 3, pp. 141-157.